Adrenomedullin promotes interneuron migration in a dual human model for hypoxic interneuronopathy of prematurity

Wojciech P. Michno[1,#], Alyssa Puno[1,#], Li Li[1], Amanda Everitt[2], Kate McCluskey[2], Fikri Birey[3,4], Saw Htun[1], Dhriti Nagar[1], Yuqin Dai[5], Emily Gurwitz[1], A. Jeremy Willsey[2, 6], Anca M. Pasca[1,*]

[1] Department of Pediatrics, Stanford University, Stanford, CA, USA

[2] Department of Psychiatry and Behavioral Sciences, UCSF Weill Institute for Neurosciences, University of California, San Francisco, San Francisco, CA, USA

[3] Department of Psychiatry and Behavioral Sciences, Stanford University, Stanford, CA, USA

[4] Stanford Brain Organogenesis, Wu Tsai Neurosciences Institute, Stanford University, Stanford, CA, USA

[5] Sarafan ChEM-H, Stanford University, Stanford, CA, USA

[6] Quantitative Biosciences Institute (QBI), University of California, San Francisco, San Francisco, CA, USA.

[#] co-first authors

* Corresponding author: apasca@stanford.edu

SUMMARY

Extremely preterm born individuals at < 28 postconceptional weeks (PCW) are at high risk for encephalopathy of prematurity and life-long neuropsychiatric conditions. Clinical studies and animal models of preterm brain injury suggest that encephalopathy of prematurity is strongly associated with exposure to hypoxia and/or inflammation in the perinatal period. Histologic examination of postmortem brain tissue from children born preterm demonstrates decreased numbers of cortical GABAergic interneurons in the cerebral cortex. However, the cellular and molecular mechanisms underlying the decreased numbers of GABAergic interneurons in the cerebral cortex of extremely preterm individuals remain unclear. Here, we developed a dual, complementary human cellular model to study hypoxia-induced interneuronopathies using human forebrain assembloids (hFA) derived from human induced pluripotent stem cells (hiPSCs) and *ex vivo* human prenatal cerebral cortex at mid-gestation. The hFA are generated through the integration of region-specific neural organoids containing either dorsal forebrain (excitatory) glutamatergic neurons or ventral forebrain (inhibitory) GABAergic interneurons. We discover a substantial reduction in migration of cortical interneurons during exposure to hypoxic stress in both hFA and *ex vivo* human prenatal cerebral cortex. Next, we identify that this migration defect is restored by supplementation of hypoxic cell culture media with exogenous adrenomedullin (ADM), a peptide hormone member of the calcitonin gene related peptide (CGRP) family. Lastly, we demonstrate that the rescue is mediated through increased activity of the PKA molecular pathway and increased pCREB-dependent expression of GABA receptors. Overall, these findings provide important insights into the cellular mechanisms contributing to cortical interneuron depletion in preterm infants, and pinpoint novel therapeutic molecular pathways with high translational potential for hypoxic encephalopathy of prematurity.

INTRODUCTION

Encephalopathy of prematurity represents the leading risk factor for epilepsy and childhood-onset neuropsychiatric diseases, including autism spectrum disorders (ASD) and attention deficit hyperactivity disorder (ADHD)[1–3]. The prevalence of neuropsychiatric diseases is highest in individuals born extremely preterm at < 28 postconceptional weeks (PCW) and correlates with the degree of prematurity[4]. While the pathophysiology of encephalopathy of prematurity is complex, clinical studies identify perinatal hypoxic events as one of the most important environmental risk factors in the perinatal period, along with inflammation[5,6].

Developmental injury of cortical interneurons is increasingly recognized as a major contributor to the pathophysiology of neuropsychiatric diseases associated with encephalopathy of prematurity[7,8]. This is intriguing for at least three main reasons: (i) the second half of in utero human prenatal brain development corresponds to the peak timing of migration of cortical interneurons from the medial ganglionic eminences

(MGE) into the dorsal forebrain[9–11], (ii) histological studies show a significant decrease in the number of cortical interneurons within the cerebral cortex of individuals born extremely premature[12–14], and (iii) perinatal episodes of hypoxia and/or inflammation are most common in extremely preterm infants. However, the molecular mechanisms underlying the depletion of cortical interneurons have been challenging to study in the developing human brain.

In this study, we investigated the effects of hypoxia on interneuron migration, using human forebrain assembloids (hFA) derived from human induced pluripotent stem cells (hiPSCs)[15–17]. To do this, we developed two complementary human cellular models for hypoxic interneuronopathies consisting of an (i) *in vitro* human cellular platform, and an (ii) *ex vivo* human prenatal cerebral cortex model. We used human forebrain assembloids (hFA) generated through the integration of region-specific human cortical organoids (hCO) and human subpallial organoids (hSO) derived from hiPSCs[15–17], and mid-gestation sections of *ex vivo* human prenatal cerebral cortex. We specifically focused on MGE-derived interneurons, which we fluorescently tagged with a cell-type specific lentiviral reporter (Dlxi1/2b::eGFP)[16,18].

Using real-time confocal live imaging of migrating GABAergic interneurons, we identify substantial migration deficits in human cortical interneurons exposed to hypoxia both in hFA and *ex vivo* sections of human prenatal cerebral cortex at ~20 PCW.

Next, we use RNA-sequencing in hypoxic hSOs to identify increased expression of adrenomedullin peptide and demonstrate that exogenous administration of adrenomedullin (ADM) peptide is sufficient to restore the baseline migration patterns of cortical interneurons exposed to hypoxia in hFA and *ex vivo* human prenatal cerebral cortex. Moreover, we use scRNA-sequencing to describe for the first time the cell type-specific expression of ADM peptide[19,20] under baseline and hypoxic conditions in human forebrain cells. We identify that under hypoxic conditions, (i) ADM expression is primarily increased in choroid plexus cells, neural progenitors and astrocytes, while (ii) expression of ADM receptors (RAMP2 in this case) increases in GABAergic and glutamatergic neurons.

Lastly, we identify that one of the molecular mechanisms of rescue by ADM in hypoxic migrating interneurons is through the activation of the cAMP/PKA/pCREB pathways with subsequent increased expression of GABA receptors, which have been previously demonstrated to modulate migration of GABAergic interneurons[21–23].

Overall, in this study we demonstrate a putatively novel role of ADM in promoting interneuron migration under hypoxic conditions, bring important insight into the biology of ADM in the cerebral cortex, and suggest a previously unexplored therapeutic avenue for hypoxic encephalopathy of prematurity and other hypoxic brain injuries.

RESULTS

Development of a human cellular model to study the migration patterns of cortical interneurons exposed to hypoxia.

The hFA recapitulate key developmental aspects of cortical interneurons migration from the ganglionic eminences into the dorsal forebrain[16,17]. To study the effects of hypoxia on the migration of human cortical interneurons, we established a model for hypoxic injury using hFA (Figure 1a). Using standardized published protocols we previously described, we generated hFA through the differentiation of hiPSCs into human cortical organoids (hCO) containing dorsal forebrain excitatory neurons, and human subpallial organoids (hSO) containing ganglionic eminence GABAergic interneurons[15–17,24,25]. To visualize migrating cortical interneurons, we fluorescently tagged cells within hSO with a MGE cell-type specific lentiviral reporter (Dlxi1/2b::eGFP)[16,18]. Subsequently, we fused labeled hSO with hCO to generate hFA. At approximately 10-14 days after fusion into hFA, we observed substantial migration of Dlxi1/2b::eGFP$^+$ cortical interneurons within the hCO side of hFA (Extended Figure 1a).

To monitor the migration patterns of cortical interneurons under hypoxic stress, we established a long-term live imaging microscopy setup in intact hFA using a confocal microscope with a motorized stage (Zeiss LSM 980 with Airyscan 2) equipped with an environmentally-controlled chamber (37ºC, 5% CO_2) and an oxygen level controller. The hFA were transferred to the confocal in a glass-bottom 96-well plate with fresh cell culture media. We imaged individual Dlxi1/2b::eGFP-tagged interneurons for a total of 48 hrs: 24 hrs (0-24 hrs) under control conditions (37ºC, 5% CO_2, 21% O_2) followed by 24 hrs (24-48 hrs) in pre-equilibrated hypoxic media (37ºC, 5% CO_2, 94.5% N_2, <1% O_2) (Figure 1a).

To validate the decrease in partial pressure of O_2 in the culture media in hypoxic conditions, we used an oxygen optical microsensor OXB50 (50 µm, PyroScience) attached to a fiber-optic multi-analyte meter (FireStingO_2, PyroSciences) and measured a media PO_2 level of ~150 mmHg in control 21% O_2 conditions, and a decrease to ~25-30 mmHg in <1% O_2 in the confocal microscope environmental chamber (Extended Figure 1b). These measurements align with our previous report, where we already demonstrated that under control conditions, PO_2 of ~150mmHg translates to ~60-80 mmHg within the hCOs[26]. Next, we confirmed that these conditions were sufficient to induce hypoxia in hSO within 24 hrs of exposure by using targeted transcriptional analyses for hypoxia-responsive genes, including *PFKP* (two-tailed paired *t*-test, P=0.004), *PDK1* (two-tailed paired *t*-test, P=0.001), *VEGFA* (two-tailed paired *t*-test, P=0.003) (Extended Figure 1c, Extended Table 2). Last, we validated the expression of HIF1a hypoxia-marker protein using western blot analyses in hSO derived from 4 individual cell lines (two-tailed paired *t*-test, P=0.01) (Extended Figure 1d, e).

Human cortical interneurons display migration deficits during exposure to hypoxia.

The migration of cortical interneurons from the ganglionic eminences into the dorsal forebrain is at its peak during the second half of pregnancy in humans[11]. It is characterized by repetitive cycles of nuclear saltations (nucleokinesis events) in the direction of the leading process (Figure 1b)[10,27]. To study migration patterns during exposure to hypoxia, we followed the movement of individual Dlxi1/2b::eGFP$^+$ cortical interneurons for 24 hrs under control conditions, followed by another 24 hrs in hypoxic conditions (Figure 1c). We identified a ~58% decrease in the number of saltation events of individual cells (paired Wilcoxon test, P<0.0001) and demonstrated that the phenotype is present in hFA derived using hiPSCs from subjects with 4 different genetic backgrounds (two-tailed paired *t*-test, P=0.003) (Figure 1d). We did not, however, observe any changes in the average length of saltation of cells when analyzed by individual cells (paired Wilcoxon test, P=0.29) and by hiPSC line (two-tailed paired *t*-test, P=0.15) (Figure 1e). In addition, we did not observe any differences in the directionality of migration measured by the ratio of euclidean/accumulated distance when analyzed by individual cells (paired Wilcoxon test, P=0.36) and by cell line (two-tailed paired *t*-test, P=0.47) (Figure 1f). For the analyses of the number of saltations/24hrs, we included all cells that had at least one saltation in control conditions and remained within the field of view until the end of the entire imaging experiment. For analyses of average saltation length and directionality, we only included cells that had at least one saltation under both control and hypoxic conditions and remained within the field of view until the end of the entire imaging experiment.

To validate that the migration deficit was not a result of prolonged live imaging, we analyzed the number of saltations of cortical interneurons under control conditions for a total of 48 hrs and compared the migration parameters in the first 24 hrs to the last 24 hrs. We identified no difference in the total number of saltations/24 hrs when analyzed by individual cells (paired Wilcoxon test, P=0.09), and hiPSC line (two-tailed paired *t*-test, P=0.2) (Figure 1g); no difference in average saltation length when analyzed by individual cells (two-tailed paired *t*-test, P=0.79), and by hiPSC line (two-tailed paired *t*-test, P=0.47) (Figure 1h); no difference in directionality of migration when analyzed by individual cells (paired Wilcoxon test, P=0.38) and by hiPSC line (two-tailed paired *t*-test, P=0.62) (Figure 1i).

Next, we checked whether re-oxygenation for 24 hrs allowed the recovery of the number of saltations/24 hrs in interneurons previously exposed to hypoxia.. To do this, we followed the movement of individual cortical interneurons for a total of 72 hrs: 24 hrs under control conditions, another 24 hrs in hypoxic conditions and 24 hrs after re-oxygenation. We found that upon re-oxygenation, the saltation deficit worsened, with ~65% decrease compared to control when analyzed by individual cells (Friedman test, P<0.0001) or hiPSC line (RM one-way ANOVA, P=0.003) (Extended Figure 1f).

Transcriptional analyses in hypoxic hSO suggest adrenomedullin peptide as a key component of hypoxia-induced response.

To investigate the transcriptional changes induced by hypoxia in hSO containing cortical interneurons, we performed bulk transcriptome-wide RNA-Sequencing (RNA-Seq) using hSO (day 46 in culture) following exposure to hypoxia for 12 hrs or 24 hrs, as well as at 72 hrs after reoxygenation (Figure 2a). For these experiments we induced hypoxia using the C-chamber hypoxia sub-chamber (Biospherix). We confirmed a significant decrease in PO_2 between control and hypoxia conditions (two-tailed paired *t*-test, $P<0.0001$) (Extended Figure 2a), and showed that PO_2 levels in both conditions were similar to the ones measured in the confocal environmental chamber (Extended Figure 1b).

Hierarchical clustering of the gene expression profiles clearly separated the hypoxia-exposed from non-exposed and reoxygenated hSO samples (Extended Figure 2b), suggesting that hypoxia exposure induces strong transcriptional profile changes in hSO, and these largely recover following 72 hrs of reoxygenation. For this experiment, we used hSO derived from 4 individual hiPSC lines, two XX and two XY genotypes (details by hiPSC line are presented in Extended Table 1).

Next, we identified differentially expressed genes (DEGs) between control, hypoxia-exposed, and reoxygenated samples (padj<0.05, fold change>1.5), controlling for potential confounding variables as described in detail in the methods section. We identified 734 differentially expressed genes at 12 hrs, 985 genes at 24 hrs, and 21 genes at 72 hrs after reoxygenation (Figure 2b, 2c, Extended Table 3).

Gene set enrichment analyses demonstrated changes in molecular pathways associated with exposure to hypoxia (including glycolysis, mTORC1, KRAS), inflammatory response pathways (represented by non-specific immune-related cell surface receptors), and estrogen response pathways. In addition, we identified changes in genes associated with general cellular migration (e.g. *AXL*, GLIPR1, etc) (Figure 2d, Extended Table 4).

Interestingly, we identified that adrenomedullin (*ADM*) gene had the highest fold change among DEGs at 24 hrs of hypoxia exposure ($\log_2FC=4.06$, padj=6.08E-19) (Figure 2e).

Single cell RNA-sequencing in hFA exposed to hypoxia uncover cell type-specific expression of ADM and its receptors.

To identify cell type-specific expression of *ADM* under control and hypoxic conditions, we performed single-cell RNA-sequencing in hSO and hCO manually separated from hFAs that were previously exposed or non-exposed to hypoxia. To do this, we manually cut the hFA under microscopic guidance. Since we wanted to capture and characterize only interneurons migrated on the hCO side and not the ones at the edge of the fusion, we intentionally performed the separation more toward the hCO side.

First, we performed Uniform Manifold Approximation and Projection (UMAP) dimensionality reduction for hSOs non-exposed (n = 8,691cells) and exposed to hypoxia (n = 7,331 cells) and identified five cell clusters (Figure 3a, Extended Figure 3a, c), including ventral forebrain progenitors and early GABAergic interneurons (*NKX2.1*$^+$, *GAD1*$^+$), cycling progenitors (*TOP2A*$^+$), astrocytes (*S100A10*$^+$) and a small cluster of radial glia (*SOX9*$^+$). As expected due to previous fusion into hFA and our experimental design for separating the hFA into hSO and hCO for scRNA-sequencing, we identified a cluster of cortical glutamatergic neurons (*STMN2*$^+$, *NEUROD2*$^+$) (Extended Figure 3c). For hCOs non-exposed (n = 6,786 cells) and exposed to hypoxia (n = 5,781cells), we also identified five cellular clusters (Figure 3b, Extended Figure 3b, d) consisting of dorsal forebrain progenitors (*SOX2*$^+$), cycling progenitors (*TOP2A*$^+$), cortical glutamatergic neurons (*STMN2*$^+$, *NEUROD2*$^+$), and a small cluster of choroid plexus cells (*TTR*$^+$). As expected due to previous fusion into hFA and migration of interneurons from the hSO side, we identified a cluster of GABAergic interneurons (*NKX2.1*$^+$, *GAD1*$^+$) (Extended Figure 3d). All these cell clusters demonstrated increased expression of hypoxia-related genes (PDK1, PKKP) (Extended Figure 3e, f).

Next, we performed subcluster analyses of GABAergic interneurons on the hSO and hCO sides, and identified that they primarily express markers for MGE and CGE including *NKX2.1*, *LHX6*, somatostatin (*SST*) or calretinin (*CALB2),* but minimal parvalbumin (*PVALB*) and neuropeptide Y (*NPY*) (Figure 3c, d, Extended Figure 3g, h, i, j).

Finally, we assessed the expression of *ADM* and its receptors (*RAMP1*, *RAMP2* and *RAMP3*) in individual cell types. We found that under control conditions *ADM* is expressed in astrocytes and choroid plexus cells, but not in other cell types. Under hypoxic conditions, the expression of *ADM* increased in choroid plexus cells, astrocytes, and dorsal and ventral forebrain progenitor cells (cycling and non-cycling) (Figure 3e, f - left). For *RAMP* receptors, we observed no expression of *RAMP2* under control conditions but increased expression in hypoxic GABAergic and glutamatergic neurons, choroid plexus and ventral cycling progenitors (Figure 3e, f - right), baseline expression of *RAMP1* under control conditions in cycling progenitors and astrocytes but no change in hypoxia (Figure 3g, h - left) and lack of expression of *RAMP3* under control and hypoxic conditions (Figure 3g, h - right).

Exogenous administration of ADM peptide during exposure to hypoxia rescues the migration deficits of human cortical interneurons.

To confirm the increase in gene expression level of *ADM* under hypoxic conditions observed in RNA-Sequencing experiments, we performed qPCR analyses using hypoxia-exposed hSO. We validated the significant transcriptional upregulation of *ADM* gene expression (two-tailed paired *t*-test, P=0.02) (Figure 4a).

To check whether the transcriptional upregulation of *ADM* gene expression translates into changes at a protein level, we measured the concentration of ADM peptide by quantitative EIA (Phoenix Pharmaceuticals, EK-010-01) in cell culture media from hSO exposed and non-exposed to hypoxia for 24 hrs. We observed ~25 fold increase in the protein concentration in the hypoxia-exposed hSO compared to control conditions (unpaired Mann-Whitney U, P<0.0001) (Figure 4b). This experiment was performed on 3 separate biological replicates of hSO, each derived from 4 hiPSC lines in one differentiation experiment (details by hiPSC line are presented in Extended Table 1).

Next, we investigated whether ADM peptide contributes to the migration of cortical interneurons. To confirm that administration of ADM does not induce changes in migration under control conditions, we analyzed the number of saltations of cortical interneurons under control conditions for a total of 48 hrs: 24 hrs under control conditions, followed by 24 hrs in control + ADM. We identified no difference in the total number of saltations/24 hrs when analyzed by individual cells (paired Wilcoxon test, P=0.23), and hiPSC line (two-tailed paired *t*-test, P=0.77) (Extended Figure 4a); no difference in average saltation length when analyzed by individual cells (two-tailed paired *t*-test, P=0.44), and by hiPSC line (two-tailed paired *t*-test, P=0.66) (Extended Figure 4b); no difference in directionality of migration when analyzed by individual cells (paired Wilcoxon test, P=0.83), and by hiPSC line (two-tailed paired *t*-test, P=0.47) (Extended Figure 4c).

To investigate the rescue potential of ADM under hypoxic conditions, we exposed hFA to hypoxia in the presence of 0.5 μM human ADM (Anaspec, AS-60447) (Figure 4c) and imaged individual migrating cortical interneurons (Figure 4d). We again observed a significant decrease in the number of saltations hypoxic conditions when analyzed by individual cells (paired Wilcoxon test, P<0.0001) and by hiPSC line (two-tailed paired *t*-test, P=0.02), and identified rescue of the number of saltations in hypoxia + ADM condition when analyzed by individual cells (paired Wilcoxon test, P=0.3) and by hiPSC line (two-tailed paired *t*-test, P=0.9) (Figure 4e). Furthermore, we found no changes in average saltation length in control versus hypoxia when analyzed by individual cells (Wilcoxon test, P=0.81), and by hiPSC line (two-tailed paired *t*-test, P=0.35); nor in control versus hypoxia + ADM when analyzed by individual cells (paired Wilcoxon test, P=0.06), and by hiPSC line (two-tailed paired *t*-test, P=0.82) (Extended Figure 4d). Lastly, we found a minor change in saltation directionality in control versus hypoxia conditions when analyzed by individual cells (Wilcoxon test, P<0.001), but no difference when analyzed by hiPSC line (two-tailed paired *t*-test, P=0.15); also no differences in control versus hypoxia + ADM when analyzed by individual cells (paired Wilcoxon test, P=0.14), and by hiPSC line (two-tailed paired *t*-test, P=0.31) (Extended Figure 4e).

Next, we checked whether administration of ADM during hypoxia rescues the saltation phenotype we previously observed in the first 24 hrs of the re-oxygenation. For this, we followed the movement of

individual cortical interneurons for a total of 72 hrs: 24 hrs under control conditions, another 24 hrs in hypoxic conditions + ADM, and 24 hrs after re-oxygenation. We found that upon re-oxygenation, the saltation deficit partially recovered in cells treated with ADM, with ~35% decrease compared to control when analyzed by individual cells (Friedman test, P<0.0001) or hiPSC line (one-way ANOVA, P=0.12), and further validated the rescue by ADM in hypoxic conditions (Figure 4f). This is much improved from hypoxic conditions where ADM was not used (Extended Figure 1f) and where the saltation decrease was ~65% from baseline.

To verify that the saltation rescue by ADM is directly linked to the administration of exogenous ADM peptide, we next imaged migrating hypoxia + ADM cortical interneurons in the presence or absence of 10 ⌠M adrenomedullin fragment 22-52 (ADM_{22-52}) (Cayman Chemical Company 24892), a specific RAMP2/3 ADM receptor blocker (Figure 4g). We further validated the saltation deficit in hypoxia and the rescue by ADM, and found that the addition of ADM_{22-52} to the hypoxia + ADM condition was sufficient to prevent the saltation rescue when analyzed in individual cells (paired Wilcoxon test, P<0.0001) and by hiPSC line (paired *t*-test test, P=0.003) (Figure 4h).

Lastly, we checked whether structural disruption of ADM affects the ability of the peptide to rescue the saltation phenotype. The key motif responsible for receptor binding and activity consists of six amino acid ring structure resulting from the disulfide-bond bridge formation between Cys16 and Cys21[28]. These post-translational modifications happen within the endoplasmic reticulum (ER), and are relevant because we identified significant transcriptional dysregulation in genes associated with ER function in our RNAseq data (e.g. upregulation of the unfolded protein response pathway (Figure 2d)) and because the formation of di-sulfide bonds is oxygen dependent[29]. To check whether the rescue by exogenous ADM is directly related to the presence of the di-sulfide bond and further validate the direct role of ADM in the rescue, we denatured and alkylated the synthetic ADM using iodoacetamide resulting in lack of blockage of reduced cysteine residues at Cys16 and Cys21 (Extended Figure 4f, g). We validated that denatured ADM (dADM) does not rescue the saltation deficit under hypoxic conditions, when analyzed by individual cells (paired Wilcoxon test, P<0.0001) and by hiPSC line (paired *t*-test test, P=0.04) (Extended Figure 4h).

Proposed molecular mechanism of rescue by ADM.

To elucidate the mechanism of rescue by ADM, we performed enzyme-immunoassays (EIA) analyses focused on cAMP/PKA, AKT/pAKT and ERK/pERK pathways, which have been previously shown to be modulated by ADM[19,20,30]. We found that the concentration of cAMP is not affected by hypoxia, but is increased in the hypoxia + ADM conditions both when analyzed by individual samples (one-way ANOVA test, P=0.0007), and by hiPSC line (one-way ANOVA test, P=0.002) (Figure 5a). These

results were complemented by increased PKA activity in hypoxia + ADM conditions when analyzed by individual samples (one-way ANOVA test, P<0.0001), and by hiPSC line (one-way ANOVA, P<0.0001) (Figure 5b). In contrast, the ratio of pAKT/AKT was decreased in hypoxia samples when analyzed by individual samples (one-way ANOVA, P<0.0001) and by hiPCS line (Kruskal-Wallis test, P=0.01), but was not rescued in hypoxia + ADM (Figure 5c). The findings were similar for the ratio of pERK/ERK in individual samples (one-way ANOVA test, P=0.001) and by hiPCS line (one-way ANOVA, P=0.02) (Figure 5d). Next, we quantified the ratio of pCREB/CREB which is downstream of all these pathways. We found that hypoxia induced a decrease in the ratio of pCREB/CREB when compared to control when analyzed by individual samples (one-way ANOVA test, P=0.003) and by hiPSC line (P=0.048). However, this ratio was restored in hypoxia + ADM conditions when analyzed by individual samples (one-way ANOVA test, P=0.27) or by hiPSC lines (one-way ANOVA, P=0.6) (Figure 5e).

Previous reports demonstrated that increased ratio of pCREB/CREB is directly involved in increasing the expression of GABA receptors, which in turn, facilitate interneuron migration. To check this, we quantified the expression of several GABAergic receptors in the presence or absence of ADM during hypoxia exposure. We found a significant decrease in expression in hypoxic conditions, but rescue in hypoxia + ADM for several GABA receptors including GABRA1 (one-way ANOVA test; control vs hypoxia: P=0.002; control versus hypoxia + ADM: P=0.17), GABRG2 (one-way ANOVA test; control versus hypoxia: P=0.007; control versus hypoxia + ADM: P=0.23), GABRB3 (Kruskal-Wallis test; control versus hypoxia: P=0.02; control versus hypoxia + ADM: P=0.05), GABRG3 (one-way ANOVA test; control versus hypoxia: P=0.01; control versus hypoxia+ADM: P=0.1) (Figure 5f, Extended Figure 5a). However, we observed no change in expression for GABRA2 (one-way ANOVA; control versus hypoxia: P=0.8; control versus hypoxia + ADM: P=0.75) and GABRB2 (Kruskal-Wallis test; control versus hypoxia: P=0.08; control versus hypoxia + ADM: P=0.25) (Extended Figure 5b). While there is only partial (yet statistically significant) rescue of expression for these receptors, they do complement each other functionally. This is the likely reason why partial increase in multiple GABAergic receptor subtypes is sufficient to achieve a minimal threshold required for increased nuclear saltation under hypoxic conditions in the presence of exogenous ADM.

Overall, we propose that one of the mechanisms of rescue by exogenous ADM supplementation is through activation of the cAMP/PKA pathway and increased ratio of pCREB/CREB, followed by increased expression of multiple GABA receptors and subsequent stimulation of saltation frequency. Schematic representation of the proposed mechanism is presented in Figure 5g.

***Ex vivo* human prenatal cerebral cortex model confirms the migration deficits and phenotypic rescue by ADM.**

To verify our findings in an independent human model for hypoxia-induced developmental interneuronopathies, we used *ex vivo* primary human cortical tissue at ~20 PCW and followed a similar experimental design used for hFA (Figure 6a). First, we sectioned human cerebral cortex sections (Figure 6b) into 400 µm slices and cultured them on live imaging-compatible cell culture inserts (diameter, 23.1 mm; pore size, 0.4 µm; Falcon, 353090)[16]. To visualize migrating cortical interneurons, we fluorescently tagged interneuron lineage cells using the cell-type specific lentiviral reporter Dlxi1/2b::eGFP (Figure 6c) which tags MGE derived interneurons[18]. Using previously published scRNA-sequencing data from mid-gestation human fetal tissue, we performed subcluster analyses in GABAergic interneurons[16,31]. We identified three subclusters. One small subcluster expressed doublets and was excluded from subsequent analyses (Extended Figure 6a)[32]. The remaining two sub-clusters were found to express MGE- and CGE-derived markers consisting of NKX2.1, LHX6, CALB2, SST (Figure 6d, e), but minimal CALB1 and *PVALB* (Extended Figure 6b), similar to the ones in hFA.

To assess whether exposure to hypoxia is sufficient to induce a migration deficit in *ex vivo* human cortical interneurons as observed in hFA, we employed the live-imaging setup established for hFA (Zeiss LSM 980 with Airyscan 2) and monitored the migration patterns of the Dlxi1/2b::eGFP^{+}-tagged interneurons for 24 hrs under control conditions (37°C, 5% CO_2, 21% O_2). We then transitioned the sections into pre-equilibrated hypoxic media (37°C, 5% CO_2, 94.5% N_2, <1% O_2) and imaged the same cells for another 24 hrs. We confirmed the transcriptional increase in *ADM* gene by qPCR (two-tailed unpaired *t*-test, P=0.0005) (Figure 6f) similar to hypoxic hSO. Following exposure to hypoxia for 24 hrs, we identified ~55 % decrease in the number of saltations (paired Wilcoxon test, P<0.0001). This was rescued by the addition of 0.5 µM ADM peptide (paired Wilcoxon test, P=0.09) (Figure 6g). We did not observe any changes in the average saltation length of individual cells in control versus hypoxia conditions (paired Wilcoxon test, P=0.88 or in the presence of ADM during the exposure to hypoxia (two-tailed paired *t*-test, P=0.37) (Figure 6h). Moreover, we observed no change in directionality in control versus hypoxia conditions (Wilcoxon test, P=0.3) nor in control versus hypoxia+ADM conditions (Wilcoxon test, P=0.8) (Figure 6i).

DISCUSSION

Accumulating evidence demonstrates the power of human cellular models for the study of neurodevelopmental diseases of genetic or environmental etiology, including tuberous sclerosis, Timothy syndrome, 22q11.2 deletion syndrome, ZikV exposure, and preterm birth. [33–38]

Here, we establish two complementary human models to study hypoxic injury in migrating human cortical interneurons using hiPSC-derived human forebrain assembloids (hFA) and *ex vivo* human prenatal cerebral cortex. We demonstrate a substantial saltation deficit of human cortical interneurons exposed to hypoxia, with no change in average saltation length or directionality. Importantly, we identify adrenomedullin (ADM) peptide as an effective pharmacological rescue for this phenotype, characterize the cell type specific expression of ADM and its receptors in multiple cell types and propose a molecular mechanism of protection of interneurons saltations by ADM under hypoxic conditions.

There are multiple novel aspects of this study, with possible implications for developmental neurobiology, hypoxia induced prematurity-associated interneuronopathies, and development of effective clinical therapies for encephalopathy of prematurity.

First, we use hFA - an innovative and newly developed hiPSC-based platform that recapitulates key features of the migration of cortical interneurons from the ganglionic eminences into the dorsal forebrain. To our knowledge, this is the first model for hypoxia-induced interneuronopathies to directly image the migration patterns of human cortical interneurons under hypoxic stress and to use two separate disease models, including hFA and *ex vivo* human prenatal cortical tissue.

Second, we demonstrate that hypoxia induces a substantial migration deficit in human cortical interneurons through reduced number of saltations, but preserved average saltation length and directionality. This finding is interesting and we speculate that the structural nucleokinesis machinery remains intact while pro-migratory signals are impaired following hypoxia. This hypothesis is supported by the novel and surprising finding that ADM, a peptide hormone from the CGRP family, pharmacologically rescues the migration deficit when supplemented in the culture media during the hypoxic insult.

Third, our study is the first to describe the cell-type specific expression of ADM and its receptors in cortical brain cells under control and hypoxic conditions. This new knowledge brings insight into the biology of ADM within the brain, and is important because ADM was historically thought to be only a by-product of vascular injury during episodes of hypoxia and inflammation. However, it is becoming increasingly studied as a protective compound for sepsis and neuroprotection[20,39–44].

Lastly, we bring evidence and speculate that exogenous administration of ADM might be required for hypoxic neuroprotection, due to known abnormal endoplasmic reticulum function during hypoxia[37,45]

and need for oxygen for proper protein folding[29]. In order to bind to its receptors and exert its biological activity, ADM requires processing in the endoplasmic reticulum for the formation of a di-sulfide bond between Cys16 and Cys21. Based on our results showing rescue by exogenous ADM and lack of rescue by denatured ADM, we speculate that the secretion of biologically active ADM in response to hypoxia is potentially blunted and the possible neuroprotective properties are attenuated. Future *in vivo* and clinical studies are needed to validate these findings and speculations.

Our study has several limitations. The hFA are especially powerful to study cell-autonomous characteristics and specific cell-cell interactions, but findings require the use of orthogonal strategies for validation because the organoids do not contain all brain cell types (e.g., oligodendrocytes, microglia) and structures (e.g., vasculature, blood-brain barrier). Here, we recapitulated the hypoxia-induced susceptibility of migrating cortical interneurons using *ex vivo* human prenatal cortical tissue exposed to the same experimental conditions. However, we did not study the effects of inflammation, the other important environmental risk factor for defects in interneuron migration. GSEA analyses from our RNAseq data in hypoxic hSO, show the presence of an "inflammatory response" module, but this is represented by non-specific immune-related cell surface receptors. The role of inflammation through direct cytokine release should be investigated in a separate study.

Separately, concerns have been raised about the high O_2 levels measured *in vitro* cultures versus *in vivo*. Clinical and *in vivo* preclinical studies demonstrate that tissue PO_2 is not a direct indicator of cellular oxygenation status. For example, it is well established that O_2 delivery to the prenatal tissues (including the brain) is significantly more efficient than following birth, despite much lower PO_2. This is because fetal blood has a high O_2 content, due to very high concentration of fetal hemoglobin and high affinity of fetal hemoglobin for O_2. This is supported by data showing the absence of markers for hypoxia in fetal brain tissue during the majority of in utero development, even if PO_2 is < 30 mmHg. Our previous *in vitro* studies show that PO_2 levels at the surface of organoids are ~80 mmHg in control conditions (21% O_2, PO_2~150mmHg), and these oxygen levels are accompanied by stable markers of cellular stress in long-term cultures[37,46,47]. On the other hand, we observe significant induction of hypoxic and stress markers at PO_2 < 30 mmHg[37]. All this data imply that oxygen level requirements are different for *in vitro* and *in vivo* studies of hypoxia, and that our model is well suited to study the effects of hypoxia on cortical development.

Lastly, for this study, we focused exclusively on the acute effects of hypoxia on the migration of immature, cortical interneurons. At this time point, our organoid cultures and ex vivo human fetal tissue contain primarily calretinin and somatostatin interneurons subtypes, but not parvalbumin. To provide additional mechanisms for the reported interneuron reduction in the cortex of preterm infants, future studies should evaluate for defects in (i) proliferation of ventral progenitors and (ii) survival and function of specific

subtypes of mature interneurons already integrated into the excitatory synaptic networks at the time of the hypoxic insult.

Along with previous disease models using human cellular models for brain development and injury, our study further strengthens the power of this approach to identify cellular and molecular mechanisms of disease, and moves us closer to the identification of therapeutic candidates with high potential for translation into effective clinical interventions.

METHODS

Culture of hiPSCs

The hiPSC lines used in this study were validated using standardized methods we previously described[15,16,25,48]. Cultures were regularly tested for, and maintained Mycoplasma free. The differentiation experiments were performed using 4 control hiPSC lines derived from fibroblasts harvested from 4 healthy individuals (two XX and two XY). Informed consent for fibroblast collection was obtained from all individuals and this process was approved by the Stanford IRB Panel.

Generation of region-specific organoids

Brain region-specific human cortical organoids (hCO) and human subpallium organoids (hSO) were differentiated using feeder-free grown hiPSCs using validated protocols we previously reported and contributed to developing[15–17,25,47–50]. Briefly, hiPSCs were maintained in six-well plates coated with recombinant human vitronectin (VTN-N, Thermo Fisher Scientific, A14700) in Essential 8 medium (Thermo Fisher Scientific, A1517001). For differentiation, hiPSC colonies were lifted from the plates using Accutase (Innovate Cell Technologies, AT-104). Approximately 3 million cells were transferred to each well in AggreWell 800 (STEMCELL Technologies, 34815) and centrifuged at 100g for 3 minutes in hiPSC medium supplemented with ROCK inhibitor Y-27632 (EMD Chemicals). After 24 hrs, the newly-formed organoids were transferred into ultra-low-attachment plastic dishes (Corning, 430293) in Essential 6 medium (Thermo Fisher Scientific, A1516401) supplemented with dorsomorphin (2.5 µM, Sigma-Aldrich, P5499) and SB-431542 (10 µM, Tocris, 1614) and additional XAV-939 (hCO 0.5 µM, hSO: 2.5 µM Tocris, 3748). This medium was replaced daily for the first five days. On the sixth day in suspension, organoids were transferred to neural medium containing Neurobasal A (Thermo Fisher Scientific, 10888022), B-27 supplement without vitamin A (Thermo Fisher Scientific,12587010), GlutaMax (2 mM, Thermo Fisher Scientific, 35050061) and penicillin and streptomycin (100 U ml^{-1}, Thermo Fisher Scientific, 15140122). For hCO the neural medium was supplemented with the growth factors EGF (20 ng ml^{-1}, R&D Systems, 236-EG) and FGF2 (20 ng ml^{-1}, R&D Systems, 233-FB) every day until day 15, then every-other day until day 23. For hSO, we included continued supplementation with XAV-939 (2.5 µM) on days 6-23, and SHH pathway agonist SAG (smoothened agonist; 100 nM; Thermo Fisher Scientific, 566660) on days 12-23. Between days 25-43, the neural medium was supplemented with neurotrophic factors BDNF (20 ng ml^{-1}, Peprotech, 450-02) and NT3 (20 ng ml^{-1}, Peprotech, 450-03), to promote differentiation of the neural progenitors into neurons in both hCO and hSO; media change were performed every other day. After day 43 hCO and hSO were maintained in unsupplemented neural media.

Viral labeling of hSO and generation of human forebrain assembloids (hFA)

The viral infection of the hSO for visualization of migrating cortical interneurons was performed as previously described[16,38]. Briefly, at approximately 45-55 days in culture, hSO were transferred to a 24 well plate (Corning, 3474) containing 500µl on neural medium with 10µl of virus (Lenti-Dlxi1/2b::eGFP; construct reported and applied in reference)[18]. After 24 hours, 500µl of neural medium was added. On day 3, all media was removed and replaced with 1ml of neurobasal medium. The next day, hSO were transferred into fresh neural media in ultra-low attachment plates. After 5-7 days, hCO and virally-infected hSO were used to generate hFA. To do this, one hCO and one hSO were transferred together into a 1.5 ml microcentrifuge Eppendorf tube and maintained in direct contact for three days. More than 95% of hCO and hSO fused. Subsequently, hFA were carefully transferred into 24 well ultra-low attachment plates (Corning, 3474) and media changes were performed very gently every two to three days. Lentivirus construct (lenti-Dlxi1/2b::eGFP) was received as a gift from J. L. Rubenstein, and virus was generated by transfecting HEK293T cells with PEI Max (Polysciences, 24765); after 48 hrs the media was collected and ultracentrifuged at 17,000 rpm at 6°C for 1 hr.

Primary human prenatal cortex processing and viral labeling

Ex vivo human prenatal cerebral cortex at 20 PCW was obtained under a protocol approved by the Research Compliance Office at Stanford University. The tissue was processed within 4 hours after collection using a previously described protocol[16,38,48]. In brief, cortical tissue was embedded in 4% low-melting-point agarose in PBS and cut using a Leica VT1200 Vibratome at 400 µm. The sections were transferred onto cell culture membrane inserts (diameter, 23.1 mm; pore size, 0.4 µm; Falcon, 353090) and incubated in culture media (66% BME, 25% Hanks, 5% FBS, 1% N-2, 1% penicillin, streptomycin and glutamine; all from Invitrogen) and 0.66% D-(+)-Glucose (Sigma) at 5% CO_2, 37 °C with the Dlxi1/2b::eGFP lentivirus for 24 hrs. Sections were then transferred to fresh cell culture media and half media changes were performed every other day. After ~5 days in culture, Dlxi1/2b::eGFP+ cells could be detected and imaging was performed within 7-10 days in culture.

Live imaging and analyses of migration patterns of Dlxi1/2b::eGFP-tagged cortical interneurons

For imaging, hFA were transferred intact into a 96–well plate (glass-bottom, Cellvis, Catalog #: P96-0-N) in 300 µl of neural media. Imaging was performed under environmentally controlled conditions (37°C, 5% CO_2, 21% O_2) using a confocal microscope with a motorized stage (Zeiss LSM 980) and equipped with a cage incubator for temperature, gas (including O_2 levels) and humidity control (Okolab Bold Line). During each recording session, we imaged up to 12 hFA at 10X magnification, at a depth of 350-400µm, and at a rate of 20 min/frame. The imaging field was focused on the hCO side of the fusion.

Samples were imaged for 24 hrs under control conditions (37°C, 5% CO_2, 21% O_2). To induce acute hypoxia, media was carefully removed and replaced with pre-equilibrated hypoxic media. All procedures were performed in the controlled hypoxic environment of the HypoxyLab (Oxford Optronix). The field of view was readjusted to capture the previous region of interest and the same cells were imaged for an additional 24 hrs while maintaining a hypoxic environment (37°C, 5% CO_2, <1% O_2). For pharmacological rescue experiments, the pre-equilibrated hypoxic media containing the peptide Adrenomedullin (ADM) (0.5 µM, Anaspec, AS-60447) +/- 10 uM ADM_{22-52} (the RAMP2/3 receptor blocker (Cayman Chemical Company, cat. no. 24892)), were added to the hFA cell culture media during hypoxia exposure. To perform re-oxygenation experiments, media was carefully removed and replaced with pre-equilibrated control media. The field of view was readjusted to capture the previous region of interest and the same cells were imaged for an additional 24 hrs while maintaining a control environment (37°C, 5% CO_2, 21% O_2).

The imaging of migration of human prenatal Dlxi1/2b::eGFP-tagged cortical interneurons was done with the same settings as described above, with the exception of image depth being 150-200µm. Slices were kept on the cell culture inserts during imaging.

Post-acquisition analyses of cell mobility were performed using ImageJ (v:2.00-rc-69/1.52n). Individual cells were identified and followed both in control and hypoxic conditions. Analyses were performed on all cells that had at least one saltation within the first 24 hrs of imaging (control conditions) and remained visible within the field of view until the end of the imaging period (up to 72 hrs). Paired analyses of number of saltations and saltation length were performed as described in the main text. To estimate the length of individual saltations, we manually tracked and identified the swelling of the soma of Dlxi1/2b::eGFP-tagged cortical interneurons before and after saltation, and measured the distance (in µm) from the initial position to the new position. The Z-stack Alignment present in Zen 3.1 Blue Edition (Zeiss) was used to correct for minor drifts during imaging. In order to assess changes in directionality of the movement, we extracted the x and y coordinates of each cell per frame and time using the Manual Tracking plugin (ImageJ). The Chemotaxis & Migration Tool (Ibidi) was then used to calculate the Accumulated (A) and Euclidean (E) distances traveled per cell over time. Data is presented by calculating the E/A ratio. Only cells which had at least one saltation within each of the conditions were included in the analysis.

Oxygen measurements in control and hypoxic cell culture media

The O_2 tension of the media was measured using the oxygen optical microsensor OXB50 (50 µm, PyroScience) attached to a fiber-optic multi-analyte meter (FireStingO_2, PyroScience), as previously described[37]. The measurement for control and hypoxia in the C-chamber hypoxia sub-chamber (Biospherix) are presented in Extended Figure 1b and Extended Figure 2a.

Real time quantitative PCR (qPCR)

mRNA was isolated using the RNeasy Mini Kit and RNase-Free DNase set (Qiagen, 74136), and template cDNA was prepared by reverse transcription using the PowerUp SYBR Green master mix for qRT-PCR (Life Technologies, A25742). Real time qPCR was performed on a CFX384 Real time system (BioRad). Data was processed using the BioRad CFX Maestro (BioRad). Primers used are listed in Extended Table 2.

Enzyme Immunoassay

The competitive enzyme immunoassay for human ADM (Phoenix Pharmaceuticals, EK-010-01) was performed according to the manufacturer's recommendation. Calculations of sample concentration were performed based on peptide standard solution in the range of 0-100ng/mL using the Tecan Infinite M1000 Pro and i-control 1.10 software. The concentrations of the samples were $\log_{10}$ transformed, and concentrations of the samples were interpolated from the sigmoidal curve. Range of reliable detection was between 0.01-100 ng/mL. Samples with concentration <0.01ng/mL were quantified as 0 in the bar plot from Figure 4b. The quantification of the pAKT:AKT(pS473) ratio and pERK:ERK (pT202/pY204, pT185/pY187) ratio was done using the AKT (Total/Phospho) InstantOne ELISA Kit (Thermo Fisher Scientific, 85-86046-11) for pAKT:AKT, and the ERK1/2 (Total/Phospho) InstantOne ELISA Kit (Thermo Fisher Scientific, 85-86013-11) for pERK:ERK. Both assays were performed according to manufacturers' protocol. For both assays, samples were lysed in 200µl lysis buffer provided by the manufacturer. Samples were incubated for 1h, and 50µl of lysate per well was used each of the assays. Quantification of cAMP levels was performed using the cAMP Assay Kit (Competitive ELISA) (Abcam, ab65355) according to manufacturers' protocol. For the analysis, samples were lysed in 250µl lysis buffer and 100µl was used for the assay. The concentration of cAMP was calculated based on the standard curve obtained from kit standards. The quantification of PKA was done using the PKA (Protein Kinase A) Colorimetric Activity Kit (Thermo Fisher Scientific, EIA PKA) according to manufacturers' protocol. For the assay, samples were lysed in 200µl lysis buffer containing protease inhibitor cocktail (1µl/mL, Sigma-Aldrich, P1860), phenylmethylsulfonyl fluoride (1mM, Sigma-Aldrich, 10837091001), and Activated Sodium Orthovanadate (10mM, Calibiochem, 567540). Samples were incubated for 1h under shaking (250rpm), and centrifuged at 10,000rpm for 10 min at 4°C. Samples were then diluted 1x with kit dilution buffer and 40ul of diluted sample was used for analysis.

Exposure of hSO to hypoxia for RNA-sequencing

At 46 days in culture, 3 hSO from 4 individual hiPSC lines were exposed to hypoxic conditions for 12 and 24 hrs using a C-chamber hypoxia sub-chamber (Biospherix) and Proox 110 Compact Oxygen

Controller (Biospherix) with a mixed CO_2/N_2 compressed gas source. For acute induction of hypoxia, the media was previously equilibrated overnight at <1% O_2, 5% CO_2, 37 °C with a resulting PO_2 of 25-30mmHg. After 12 hrs and 24 hrs of hypoxic exposure, hSO were immediately collected and snap-frozen in dry ice for analyses. Control hSO maintained in regular incubator conditions were collected from each hiPSC line at each experimental timepoint. Additionally, extra hSO exposed to 24 hrs of hypoxia were transferred back to baseline conditions and reoxygenated for 72 hrs. At this timepoint, samples were collected, matched with control hSO and snap-frozen on dry ice. All samples were kept at -80°C until they were processed for RNA-sequencing.

RNA sequencing analyses

mRNA was isolated using the RNeasy Mini kit (Qiagen) and sequence libraries were prepared by Admera Health (www.admerahealth.com) using the KAPA Hyper Prep Stranded RNA-Seq with RiboErase. Sequencing was performed on the Illumina HiSeq 400 system with paired-end 150 base pair reads. Samples averaged 40 million reads, each representing 20x genome coverage. Trimmed RNA-Seq reads were aligned to the Ensembl GRCh38 human genome reference using STAR v2.7.3 in gene annotation mode[48]. Alignment and RNA-Seq quality control metrics were generated with Picard (v 2.21.1). Principal component analysis (PCA) of the quality control matrices did not indicate any sample outliers.

Gene-level counts were filtered to remove lowly expressed genes which did not have at least 1 count per million in at least 4 out of the total 24 samples; this resulted in 17,777 remaining genes. We noticed a slight GC content bias across samples, so gene counts were further normalized by GC content, gene length, and sequencing depth using the CQN R package v1.36.0[49]. The resulting estimation parameters were provided to the negative binomial generalized linear model while performing the differential expression (DEG) analysis. This was carried out using DESeq2 v1.30.1 to identify significant genes between hypoxic conditions at each timepoint while also accounting for unwanted variation due to cell line[50]. The resulting P values were corrected for multiple comparisons using the Benjamini-Hochberg method. Genes were considered significant at FDR ≤ 0.05 and absolute fold change > 1.5 ($\log_2$FC of 0.6). In total, we identified 734 DEX genes as a consequence of the hypoxic conditions at 12 hrs, 985 genes at 24 hrs, and only 21 genes at 72 hrs after reoxygenation (Figure 2b, 2c, Extended Figure 2b, Extended Table 3). We generated the dendrogram in Figure 2b using expression data from all 24 samples, narrowed to the union of the genes differentially expressed between hypoxic and control conditions at 12 and 24 hrs or 72 hrs after reoxygenation (n = 1,473). Hierarchical clustering, using complete linkage of Euclidean distance, determined the order of the dendrogram. Z-score normalized expression values are depicted on a continuous scale from lower values (purple) to higher values (orange). The notable reduction of DEG at 72 hrs after reoxygenation reflects what we visually see in the PCA of the normalized gene expression, in that the

control and hypoxia conditions cluster together at 72 hrs post reoxygenation (not shown). Indeed, hierarchical clustering using the Ward's criterion on the first three principal components separates hypoxic samples at 12 and 24 hrs from the control 12 and 24 hrs samples as well as the reoxygenated samples (Extended Figure 2b).

To gain insight about putatively dysregulated biological pathways, we conducted gene set enrichment analysis that was computed using the fgsea R package v1.18.0 where all genes were ranked by their absolute $\log_2$ fold change[51]. We evaluated the Molecular Signatures Database "Hallmark" gene sets and supplemented the WU_cell migration set based on its presence in a preliminary gene ontology enrichment (Extended Table 4). The top 10 significantly enriched gene sets (padj < 0.05) that occur across all timepoints are shown in Figure 2d. Interested in discovering which genes had the largest change in response between 12 hrs and 24 hrs, we identified genes significant at both timepoints and ranked them by absolute difference in fold change. The top three genes increasing and decreasing in expression are shown in Figure 2e.

Single cell gene expression data collection and analyses

For single cell gene expression analyses, human forebrain assembloids (hFA) were infected with Lenti-Dlxi1/2b::eGFP as described above. Samples were incubated either under a normoxic environment (37°C, 5% CO_2, 21% O_2), or under the controlled hypoxic environment of the HypoxyLab (Oxford Optronix). Following the environmental exposure, hFA were dissected under a microscope to separate the hFA into hSO and hCO. To analyze only interneurons migrated within the hCO and not the ones still at the edges of the fusion, we intentionally performed the separation of hFA more toward the hCO side. For single cell gene expression analysis, organoids were dissociated as previously described[16,47]. Dissociated cells were resuspended in ice-cold PBS containing 0.02% BSA and loaded onto a Chromium Single cell 3′ chip (with an estimated recovery of 10,000 cells per channel) to generate gel beads in emulsion (GEMs). scRNA-seq libraries were prepared with the Chromium Single cell 3′ GEM, Library & Gel Bead Kit v2 (10x Genomics, PN: 120237). Libraries from different samples were pooled and sequenced on a NovaSeq S4 (Illumina) using 150 × 2 chemistry. Sample demultiplexing, barcode processing and unique molecular identifiers counting was performed using the Cell Ranger software suite (v6.1.2 with default settings excluding introns). Reads were then aligned to the human reference genome (GRCh38), filtered, and counted. Expression matrices for the samples were processed using the R (v4.1.2) package Seurat (v4.2). We excluded cells that express less than 2500 genes as well as those with a proportion of mitochondrial reads higher than 15%. Gene expression was then normalized using a global-scaling normalization method (normalization.method='LogNormalize', scale.factor = 10,000), and the 2,000 most variable genes were

then selected (selection.method='versust'). *Harmony* package[51] was used to integrate control and hypoxia samples for downstream analysis. The top 7 and 6 principal components for hCO and hSO samples respectively were utilized to perform a UMAP projection, implemented with the *RunUMAP* function with default settings. The clusters were generated with resolutions of 0.1 and 0.3 respectively for hCO and hSO samples using the *FindNeighbors* and *FindClusters* functions. We identified clusters based on differential expression of known markers[16,25] dentified using the FindAllMarkers function with default settings. In some cases, using expression of known markers, we grouped together clusters that were originally separate based on the Seurat clustering. For visualization purposes, the color palette of UMAP plots for hSO and hCO was adjusted using "magic wand" in non-contiguous mode for selection of all cells from respective clusters, for subsequent synchronization of the color for the given cell cluster between brain regions (Adobe Photoshop CS 2018). Original plots are available upon request. Markers used to verify the hypoxic response were based on *PDK1* and *PFKP.* Proportions of cells expressing *ADM*, *RAMP1* or *RAMP2* (Expression Level>0) out of all cells per cluster were calculated using (https://rdrr.io/github/vertesy/Seurat.utils/man/PrctCellExpringGene.html).

The top 20, 8, and 6 principal components were used to sub-cluster the GABAergic cells from hCO, hSO and HFT datasets respectively. The clusters were generated using 0.1 resolution for all three datasets. Clusters that corresponded to human GABAergic interneuron subtypes were identified based on known markers[16,31,38,49]. Doublets in the HFT dataset were identified using Doublet Finder[32]. The following parameters were used: doublet formation rate: 7.5%, PCs = 1:10, pN = 0.25, pK = 0.09. Cells with doublets were excluded from subsequent analyses.

Synthetic ADM peptide denaturation and LC-MS analysis

The synthetic peptide Adrenomedullin (ADM) (2 nmol, Anaspec, AS-60447) was incubated with either ddH_20 (for control condition) or Dithiothreitol (DTT) (5mM, Sigma Aldrich, D5545), at 56 °C for 30 min. Following reduction of disulfide bridges, alkylation of the free SH-groups was performed Iodoacetamide (IAM) (20mM, Sigma-Aldrich, I1149) at 23 °C for 45 min in the dark. The unreacted IAM was quenched with 5mM final DTT. The solution was desalted and concentrated using Amicon Ultra (3kD, EMD Millipore, UFC500324), and the volume was adjusted to the starting volume with UltraPure DNase/RNase Free Distilled Water (Thermo Fisher Scientific, 10-977-015).

LC-MS analysis was performed using Vanquish LC system coupled with an ID-X Tribrid mass spectrometry equipped with a heated electrospray ionization source (HESI-II, Thermo Scientific). For the LC system, a ZORBAX RRHD diphenyl 100 x 2.1 mm column (Agilent, 858750-944) was used. The mobile phases were 0.1% formic acid (Fisher Scientific, A117-50) in ddH_2O for A and 0.1% formic acid in acetonitrile (Sigma-Aldrich, 34998) for B. The chromatographic gradient was as follows: 0-2min 10% B,

linear increase 2-10min up to 60% B, linear increase 10-15min up to 98% B, hold 15-17min at 98% B, linear decrease 17-18min to 10% B, equilibrate 18-21min at 10% B. The mobile phase flowrate was set to 250 µl/min with an injection volume of 3 µL. The autosampler temperature was set to 4 °C, and the column chamber temperature to ambient. Data acquisition on the IDX MS was acquired at 120,000 resolution setting with positive ion voltage of 3.5kV, vaporizer and transfer tube temperature of 325 °C; AGC target set to standard, RF lens set to 45%, sheath gas set to 40 AU, aux gas set to 12 AU, maximum injection time of 100ms, with 5 microscans/acquisition, and scan range of 500-2000 *m/z*. Examination of the LC-MS data was performed using Xcalibur FreeStyle 1.6 (Thermo Scientific). Here, we monitored the formation of carbamidomethyl-cysteines at Cys16-Cys21 (predicted M+1: 6142.9973), or the reduced form of the peptide (predicted M+1: 6028.9544).

STATISTICAL ANALYSES

Data are presented as mean ±s.e.m. unless otherwise indicated. Distribution of the raw data was tested for normality; statistical analyses were performed as indicated in figure legends. Sample sizes were estimated empirically or based on power calculations. Blinding was used for analyses comparing control and treatment samples.

DATA AVAILABILITY

Gene expression data are available in the Gene Expression Omnibus (GEO) under accession number GSE183201 (token: odqhewkkrjsdzgd).

AUTHOR CONTRIBUTIONS

W.P.M. and A.P. contributed equally to the work. They performed neural differentiations, hypoxia experiments, live-imaging experiments, data analysis and contributed to experimental design and manuscript writing. A.E., K.M. A.J.W, performed data analyses for RNA-Sequencing, figure generation and contributed to manuscript writing. L.L contributed to experimental design and data collection, data analyses and designed and assembled the figures. F.B. contributed to experimental design, data collection and sc-RNA-sequencing analyses. D.N., S.H and E.G. contributed to data collection and data analyses for WB and qPCRs. Y.D. contributed to mass spectrometry data generation and analyses. A.M.P. supervised the work and wrote the manuscript with input from all authors.

COMPETING INTEREST STATEMENT

Stanford University was granted a patent that covers the generation of region-specific brain organoids and assembloids. A.M.P is listed as inventor for U.S Patent number: 10,494,602 B2. F.B is listed as inventor for U.S. Patent number 10,676,715.

ACKNOWLEDGMENTS

We thank the members of the NeoPasca lab and other collaborators for constructive feedback and or editing the manuscript (alphabetical order: Tudor Braicu, Yusuke Hori, Madison House, Geana Marte, Sherry Mestan, Sergiu P. Pasca, Deniz Yagmur Urey, Andrea Navarrette Vargas, Sam Simpson). This project was supported by Stanford Maternal & Child Health Research Institute (MCHRI) Postdoctoral Fellowship (to L. L.), Knut and Alice Wallenberg Foundation Postdoctoral Fellowship (to W.M), and Bill and Melinda Gates Foundation. Figures were created with BioRender.com.

REFERENCES

1. Volpe, J. J. The Encephalopathy of Prematurity-Brain Injury and Impaired Brain Development Inextricably Intertwined. *Seminars in Pediatric Neurology* Preprint at https://doi.org/10.1016/j.spen.2009.09.005 (2009).
2. Moster, D., Lie, R. T. & Markestad, T. Long-Term Medical and Social Consequences of Preterm Birth. *New England Journal of Medicine* **359**, 262–273 (2008).
3. Crump, C., Sundquist, J. & Sundquist, K. Preterm or Early Term Birth and Risk of Autism. *Pediatrics* e2020032300 (2021) doi:10.1542/peds.2020-032300.
4. Pierrat, V. *et al.* Neurodevelopmental outcomes at age 5 among children born preterm: EPIPAGE-2 cohort study. *BMJ* **373**, (2021).
5. Back, S. A. & Miller, S. P. Brain injury in premature neonates: A primary cerebral dysmaturation disorder? *Annals of Neurology* vol. 75 469–486 Preprint at https://doi.org/10.1002/ana.24132 (2014).
6. Penn, A. A., Gressens, P., Fleiss, B., Back, S. A. & Gallo, V. Controversies in preterm brain injury. (2016) doi:10.1016/j.nbd.2015.10.012.
7. Takano, T. Interneuron dysfunction in syndromic autism: Recent advances. *Developmental Neuroscience* Preprint at https://doi.org/10.1159/000434638 (2015).
8. Cobos, I. *et al.* Mice lacking Dlx1 show subtype-specific loss of interneurons, reduced inhibition and epilepsy. *Nat Neurosci* (2005) doi:10.1038/nn1499.
9. MF, P. *et al.* Extensive migration of young neurons into the infant human frontal lobe. *Science* **354**, (2016).
10. Mayer, C. *et al.* Developmental diversification of cortical inhibitory interneurons. *Nature Publishing Group* **555**, (2018).
11. Anderson, S. A., Eisenstat, D. D., Shi, L. & Rubenstein, J. L. R. Interneuron migration from basal forebrain to neocortex: dependence on Dlx genes. *Science (1979)* **278**, 474 LP – 476 (1997).
12. Iai, M. & Takashima, S. Thalamocortical development of parvalbumin neurons in normal and periventricular leukomalacia brains. *Neuropediatrics* **30**, 14–18 (1999).
13. Robinson, S., Li, Q., DeChant, A. & Cohen, M. L. Neonatal loss of γ–aminobutyric acid pathway expression after human perinatal brain injury. *J Neurosurg Pediatr* **104**, 396–408 (2006).
14. Lacaille, H. *et al.* Impaired interneuron development in a novel model of neonatal brain injury. *eNeuro* (2019) doi:10.1523/ENEURO.0300-18.2019.
15. Pasca, A. M. *et al.* Functional cortical neurons and astrocytes from human pluripotent stem cells in 3D culture. *Nat Methods* **12**, 671–678 (2015).

16. Birey, F. *et al.* Assembly of functionally integrated human forebrain spheroids. *Nature* (2017) doi:10.1038/nature22330.
17. Sloan, S. A., Andersen, J., Paşca, A. M., Birey, F. & Paşca, S. P. Generation and assembly of human brain region–specific three-dimensional cultures. *Nat Protoc* **13**, 2062–2085 (2018).
18. Potter, G. B. *et al.* Generation of Cre-transgenic mice using Dlx1/Dlx2 enhancers and their characterization in GABAergic interneurons. *Molecular and Cellular Neuroscience* **40**, 167–186 (2009).
19. Kitamura, K. *et al.* Adrenomedullin: A novel hypotensive peptide isolated from human pheochromocytoma. *Biochem Biophys Res Commun* (1993) doi:10.1006/bbrc.1993.1451.
20. Li, F.-J., Zheng, S.-R. & Wang, D.-M. Adrenomedullin: an important participant in neurological diseases. *Neural Regen Res* **15**, 1199–1207 (2020).
21. Heck, N. *et al.* GABA-A Receptors Regulate Neocortical Neuronal Migration In Vitro and In Vivo. *Cerebral Cortex* **17**, 138–148 (2007).
22. Cuzon, V. C., Yeh, P. W., Cheng, Q. & Yeh, H. H. Ambient GABA Promotes Cortical Entry of Tangentially Migrating Cells Derived from the Medial Ganglionic Eminence. *Cerebral Cortex* **16**, 1377–1388 (2006).
23. Manent, J. B. *et al.* A Noncanonical Release of GABA and Glutamate Modulates Neuronal Migration. *Journal of Neuroscience* **25**, 4755–4765 (2005).
24. S.A., S. *et al.* Human Astrocyte Maturation Captured in 3D Cerebral Cortical Spheroids Derived from Pluripotent Stem Cells. *Neuron* (2017) doi:http://dx.doi.org/10.1016/j.neuron.2017.07.035.
25. Yoon, S.-J. *et al.* Reliability of human cortical organoid generation. *Nat Methods* **16**, 75–78 (2019).
26. Paşca, A. M. *et al.* Human 3D cellular model of hypoxic brain injury of prematurity. *Nat Med* **25**, 784 (2019).
27. Lim, L., Mi, D., Llorca, A. & Marín, O. Development and Functional Diversification of Cortical Interneurons. *Neuron* **100**, 294–313 (2018).
28. Fischer, J. P. *et al.* Adrenomedullin disulfide bond mimetics uncover structural requirements for AM 1 receptor activation. *Journal of Peptide Science* **25**, (2019).
29. Koritzinsky, M. *et al.* Two phases of disulfide bond formation have differing requirements for oxygen. *J Cell Biol* **203**, 615–627 (2013).
30. Garelja, M. L. *et al.* Molecular Mechanisms of Class B GPCR Activation: Insights from Adrenomedullin Receptors. *ACS Pharmacol Transl Sci* **3**, (2020).
31. Schmitz, M. T. *et al.* The development and evolution of inhibitory neurons in primate cerebrum. *Nature* **603**, (2022).
32. McGinnis, C. S., Murrow, L. M. & Gartner, Z. J. DoubletFinder: Doublet Detection in Single-Cell RNA Sequencing Data Using Artificial Nearest Neighbors. *Cell Syst* **8**, (2019).
33. Blair, J. D., Hockemeyer, D. & Bateup, H. S. Genetically engineered human cortical spheroid models of tuberous sclerosis. *Nature Medicine 2018 24:10* **24**, 1568–1578 (2018).
34. Paşca, S. P. *et al.* Using iPSC-derived neurons to uncover cellular phenotypes associated with Timothy syndrome. *Nat Med* **17**, 1657–1662 (2011).
35. Qian, X. *et al.* Brain-Region-Specific Organoids Using Mini-bioreactors for Modeling ZIKV Exposure. *Cell* **165**, 1238–1254 (2016).
36. Meechan, D. W., Tucker, E. S., Maynard, T. M. & LaMantia, A. S. Diminished dosage of 22q11 genes disrupts neurogenesis and cortical development in a mouse model of 22q11 deletion/DiGeorge syndrome. *Proc Natl Acad Sci U S A* (2009) doi:10.1073/pnas.0905696106.

37. Pașca, A. M. *et al.* Human 3D cellular model of hypoxic brain injury of prematurity. *Nat Med* **25**, 784–791 (2019).
38. Birey, F. *et al.* Dissecting the molecular basis of human interneuron migration in forebrain assembloids from Timothy syndrome. *Cell Stem Cell* **29**, 248-264.e7 (2022).
39. Geven, C., Kox, M. & Pickkers, P. Adrenomedullin and Adrenomedullin-Targeted Therapy As Treatment Strategies Relevant for Sepsis. *Front Immunol* **9**, 292 (2018).
40. Pedreño, M. *et al.* Adrenomedullin protects from experimental autoimmune encephalomyelitis at multiple levels. *Brain Behav Immun* (2014) doi:10.1016/j.bbi.2013.11.021.
41. Robertson, C. L. *et al.* Increased adrenomedullin in cerebrospinal fluid after traumatic brain injury in infants and children. *J Neurotrauma* (2001) doi:10.1089/089771501750451785.
42. Miyashita, K. *et al.* The neuroprotective and vasculo-neuro-regenerative roles of adrenomedullin in ischemic brain and its therapeutic potential. *Endocrinology* (2006) doi:10.1210/en.2005-1038.
43. Kim, S.-M., Kim, J.-Y., Lee, S. & Park, J.-H. Adrenomedullin protects against hypoxia/reoxygenation-induced cell death by suppression of reactive oxygen species via thiol redox systems. *FEBS Lett* **584**, 213–218 (2010).
44. Chaung, W. W. *et al.* Peripheral Administration of Human Adrenomedullin and Its Binding Protein Attenuates Stroke-Induced Apoptosis and Brain Injury in Rats. *Molecular Medicine* **17**, 1075–1083 (2011).
45. Chavez-Valdez, R., Flock, D. L., Martin, L. J. & Northington, F. J. Endoplasmic reticulum pathology and stress response in neurons precede programmed necrosis after neonatal hypoxia-ischemia. *International Journal of Developmental Neuroscience* **48**, (2016).
46. Trevino, A. E. *et al.* Chromatin accessibility dynamics in a model of human forebrain development. *Science (1979)* (2020) doi:10.1126/science.aay1645.
47. Gordon, A. *et al.* Long-term maturation of human cortical organoids matches key early postnatal transitions. *Nat Neurosci* **24**, 331–342 (2021).
48. Dobin, A. *et al.* STAR: ultrafast universal RNA-seq aligner. *Bioinformatics* **29**, 15–21 (2013).
49. Hansen, K. D., Irizarry, R. A. & WU, Z. Removing technical variability in RNA-seq data using conditional quantile normalization. *Biostatistics* **13**, 204–216 (2012).
50. Love, M. I., Huber, W. & Anders, S. Moderated estimation of fold change and dispersion for RNA-seq data with DESeq2. *Genome Biol* **15**, 550 (2014).
51. Korotkevich, G. *et al.* Fast gene set enrichment analysis. *bioRxiv* 60012 (2021) doi:10.1101/060012.

FIGURE 1

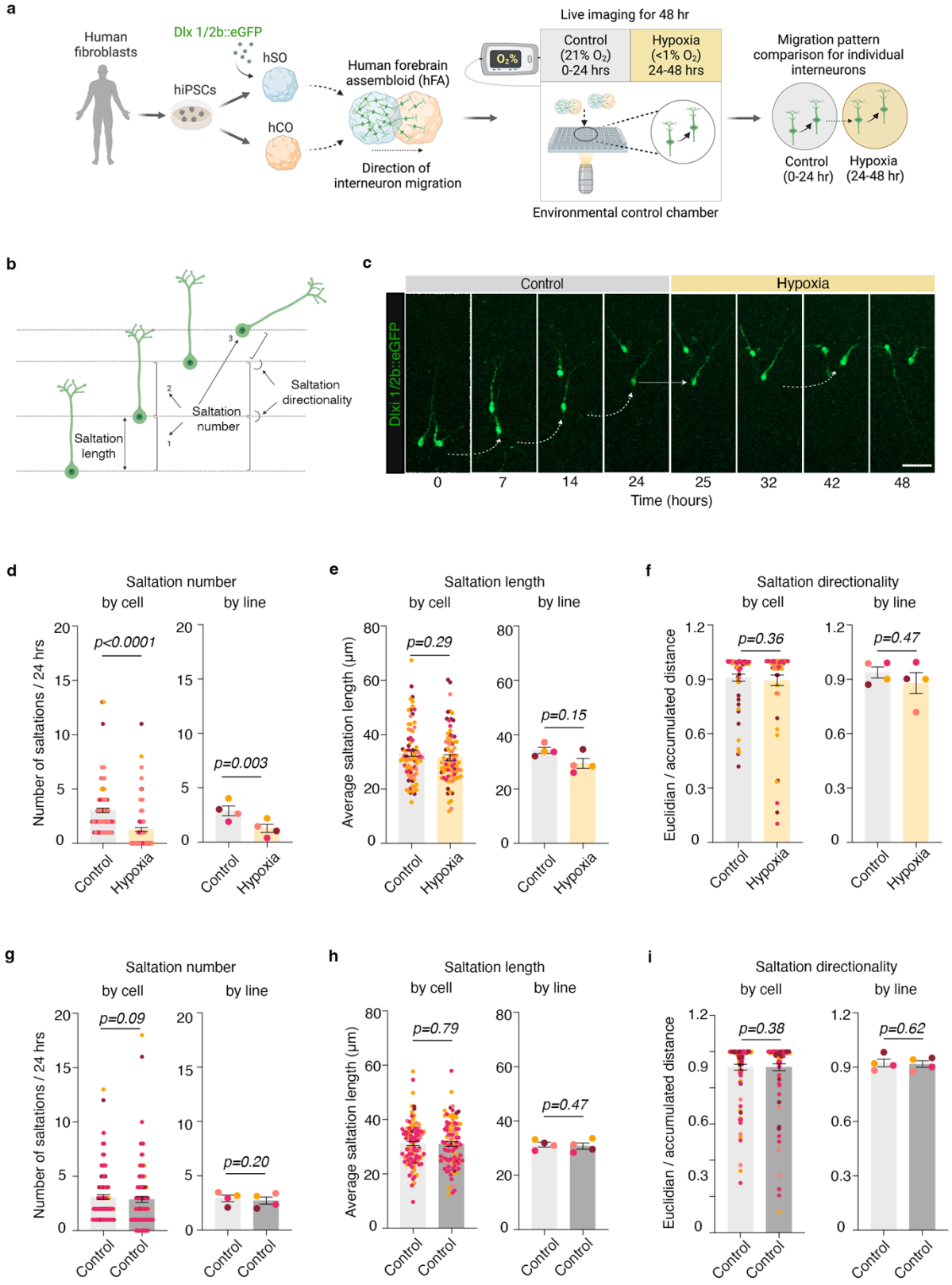
a
Human fibroblasts
Dlx 1/2b::eGFP
hiPSCs
hSO
hCO
Human forebrain assembloid (hFA)
Direction of interneuron migration
Live imaging for 48 hr
Control (21% O2) 0-24 hrs
Hypoxia (<1% O2) 24-48 hrs
Environmental control chamber
Migration pattern comparison for individual interneurons
Control (0-24 hr)
Hypoxia (24-48 hr)
b
Saltation length
Saltation number
Saltation directionality
c
Control
Hypoxia
Dlxi 1/2b::eGFP
0
7
14
24
25
32
42
48
Time (hours)
d
Saltation number
by cell
by line
Number of saltations / 24 hrs
p<0.0001
p=0.003
Control
Hypoxia
e
Saltation length
Average saltation length (µm)
p=0.29
p=0.15
f
Saltation directionality
Euclidian / accumulated distance
p=0.36
p=0.47
g
p=0.09
p=0.20
h
p=0.79
p=0.47
i
p=0.38
p=0.62

Figure 1. Human cellular model to study migration patterns in cortical interneurons under hypoxic stress.

a. Schematic illustrating overall experimental design: hiPSCs were used to derive human cortical organoids (hCO) and human subpallial organoids (hSO); for direct visualization of migrating interneurons, at ~45-55 days in culture hSO were infected with lentivirus Dlxi1/2b::eGFP and then fused with hCO into human forebrain assembloid (hFA); to study interneuron migration during exposure to hypoxia, hFA were imaged 10-14 days post infection using confocal live-imaging setup focused on the hCO part of the hFA; the movement of the same cells was followed for a total of 48 hrs, each condition for 24hrs: 0-24 hrs in control and 24-48 hrs in hypoxia; **b.** Schematic of migratory pattern of interneurons, focused on number of saltations, average saltation length and directionality; **c.** Example of migration pattern of one cortical interneuron during control and hypoxic conditions; **d.** Quantification of saltations number/24 hrs in hypoxia-exposed and non-exposed cortical interneurons by individual cells (paired Wilcoxon test, $P<0.0001$) and by hiPSC line (two-tailed paired *t*-test, $P=0.003$); **e.** Quantification of average saltation length for hypoxia-exposed and non-exposed cortical interneurons by individual cells (paired Wilcoxon test, $P=0.29$) and by hiPSC line (two-tailed paired *t*-test, $P=0.15$); **f.** Quantification of directionality of migration in hypoxia-exposed and non-exposed cortical interneurons by individual cells (paired Wilcoxon test, $P=0.36$), and by hiPSC cell line (two-tailed paired *t*-test, $P=0.47$); **g**. Quantification of saltations number/24 hrs in control conditions, in the first 24 hrs (0-24 hrs) versus the subsequent 24 hrs (24-48 hrs) of live imaging by individual cells (paired Wilcoxon test, $P=0.09$) and hiPSC line (two-tailed paired *t*-test, $P=0.2$); **h.** Quantification of average saltation length in control conditions, in the first 24 hrs (0-24hrs) versus the subsequent 24 hrs (24-48 hrs) of live imaging by individual cells (two-tailed paired *t*-test, $P=0.79$) and by hiPSC line (two-tailed paired *t*-test, $P=0.47$; **i**. Quantification of directionality of migration in hypoxia-exposed and non-exposed cortical interneurons by individual cells (paired Wilcoxon test, $P=0.38$) and by hiPSC line (two-tailed paired *t*-test, $P=0.62$);. Bar charts: mean±s.e.m; scale bar: 50 μm. Different dot colors represent individual hiPSC lines.

FIGURE 2

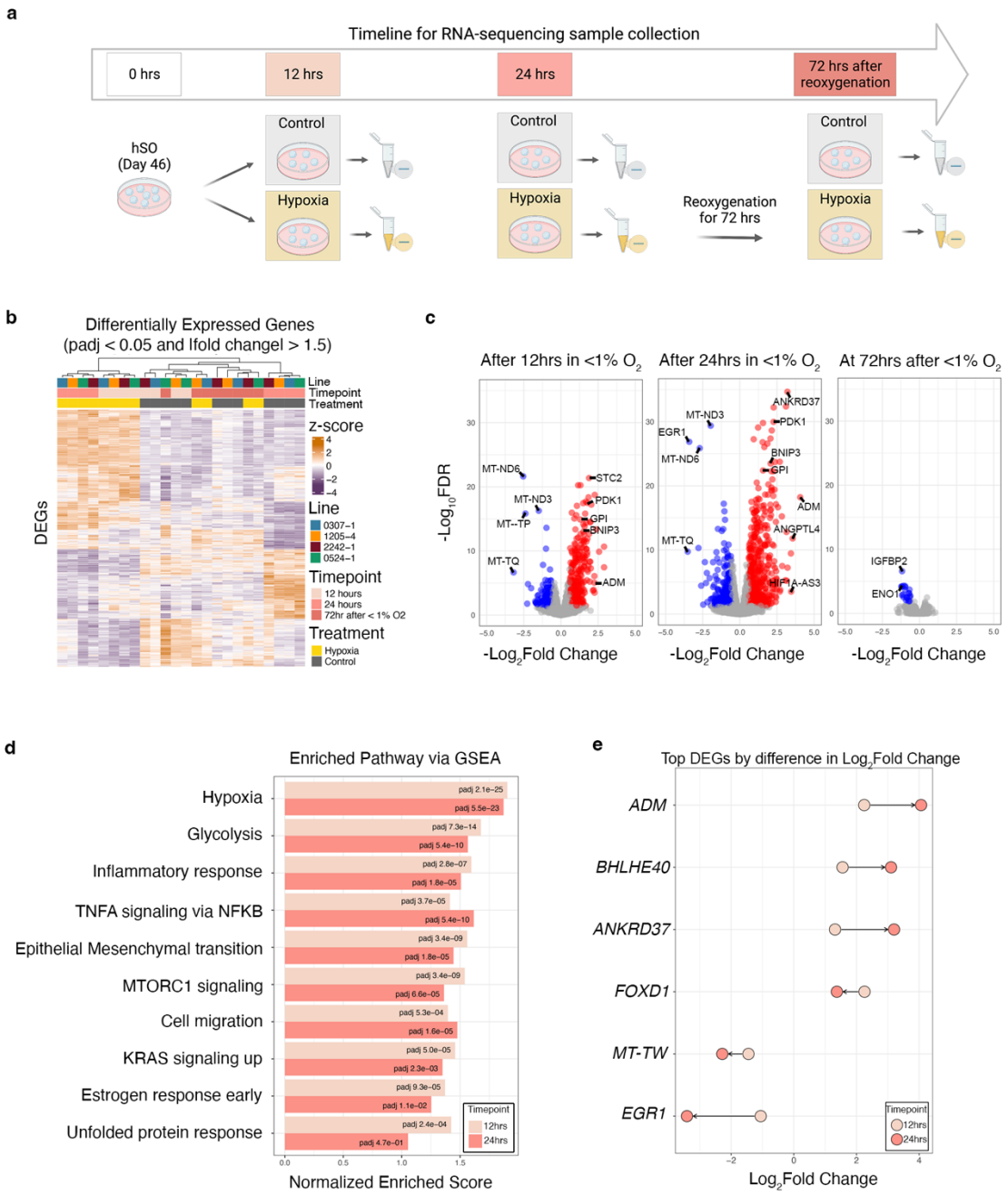
a
Timeline for RNA-sequencing sample collection
0 hrs
12 hrs
24 hrs
72 hrs after reoxygenation
hSO (Day 46)
Control
Hypoxia
Reoxygenation for 72 hrs
b
Differentially Expressed Genes (padj < 0.05 and lfold changel > 1.5)
Line
Timepoint
Treatment
z-score
DEGs
0307–1
1205–4
2242–1
0524–1
12 hours
24 hours
72hr after < 1% O2
Hypoxia
Control
c
After 12hrs in <1% O2
After 24hrs in <1% O2
At 72hrs after <1% O2
-Log10 FDR
-Log2 Fold Change
MT-ND6
STC2
MT-ND3
PDK1
MT-TP
GPI
BNIP3
MT-TQ
ADM
EGR1
ANKRD37
ANGPTL4
HIF1A-AS3
IGFBP2
ENO1
d
Enriched Pathway via GSEA
Hypoxia
Glycolysis
Inflammatory response
TNFA signaling via NFKB
Epithelial Mesenchymal transition
MTORC1 signaling
Cell migration
KRAS signaling up
Estrogen response early
Unfolded protein response
Timepoint
12hrs
24hrs
Normalized Enriched Score
e
Top DEGs by difference in Log2 Fold Change
ADM
BHLHE40
ANKRD37
FOXD1
MT-TW
EGR1
Log2 Fold Change

Figure 2. Transcriptional changes in hSO exposed to hypoxia.

a. Schematic of hypoxia exposure of hSO and collection of samples for RNA-Sequencing; **b.** Heatmap of differentially expressed genes in RNA-Seq data showing clear transcriptional changes in hypoxia-exposed samples. Samples ($n = 24$) from hSO differentiated from 4 hiPSC lines were collected at 12 hrs and 24 hrs of exposure to hypoxia, as well as 72 hrs after reoxygenation. The union of all differentially expressed genes (n = 1,473) and samples (n = 24) are ordered by hierarchical clustering (complete linkage of Euclidean distance). Z-score normalized expression values are depicted on a continuous scale from lower values (purple) to higher values (orange). Cell lines, treatment and time point are depicted at the top and represented by different colors; **c.** Volcano plots of differentially expressed genes (DEGs) at 12 hrs, 24 hrs and 72 hrs after reoxygenation. Each dot represents a single gene. DEGs with a padj<0.05 and an absolute fold change>1.5 are shown in red (upregulated) or blue (downregulated) and unchanged genes are shown in gray; **d.** Bar plot of the top 10 shared enriched gene pathways across hypoxic conditions. Adjusted p-values are depicted as text and colors represent the length of hypoxic exposure; **e.** Dumbbell plot of the top 6 DEGs with the largest positive difference and the largest negative difference in Log_2 fold change between 12 and 24 hrs of hypoxia exposure; the arrow indicates the direction of change from 12 to 24 hrs.

FIGURE 3

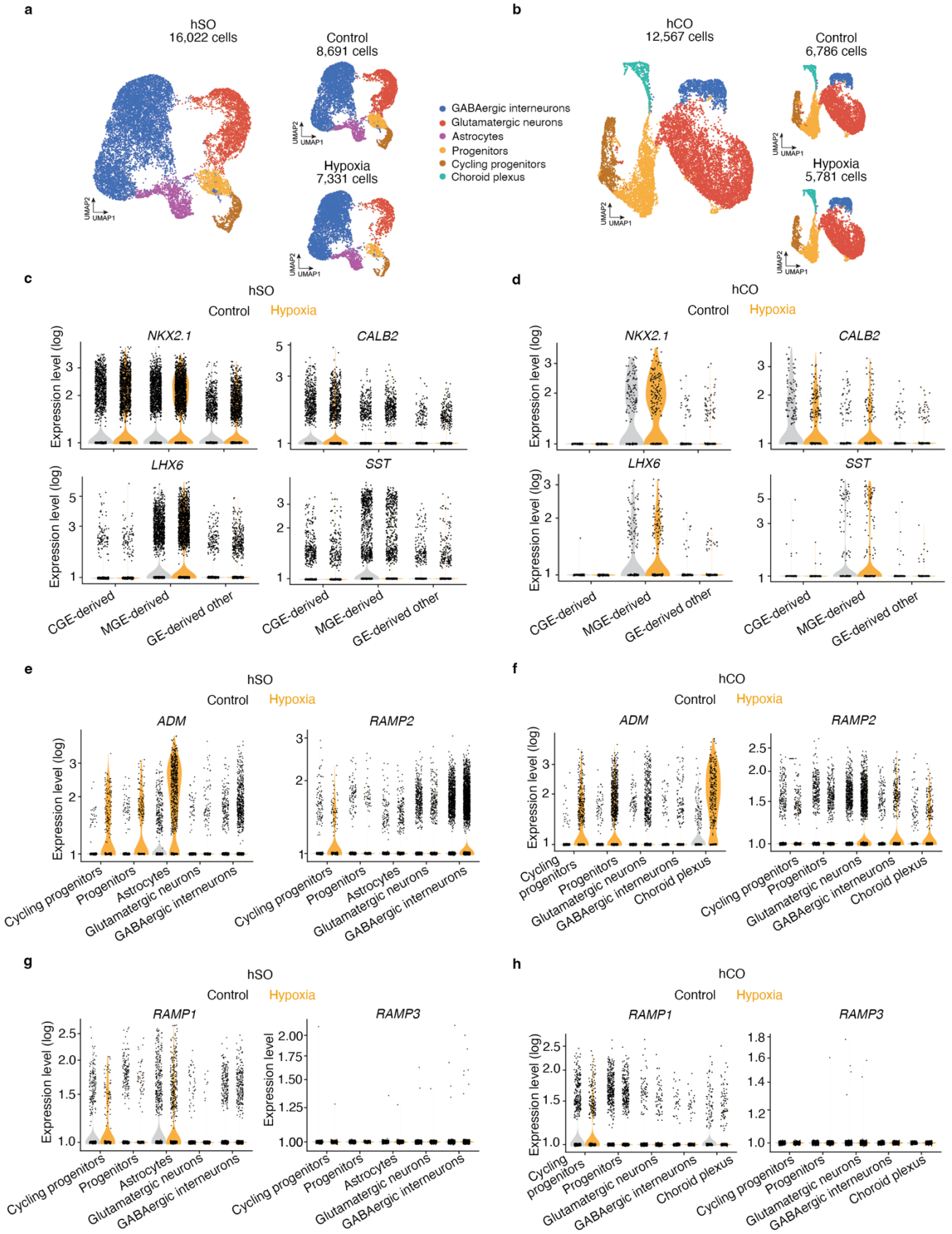
a
hSO
16,022 cells
Control
8,691 cells
Hypoxia
7,331 cells
UMAP2
UMAP1
GABAergic interneurons
Glutamatergic neurons
Astrocytes
Progenitors
Cycling progenitors
Choroid plexus
b
hCO
12,567 cells
Control
6,786 cells
Hypoxia
5,781 cells
c
hSO
Control
Hypoxia
NKX2.1
CALB2
LHX6
SST
Expression level (log)
CGE-derived
MGE-derived
GE-derived other
d
hCO
e
ADM
RAMP2
Cycling progenitors
Progenitors
Astrocytes
Glutamatergic neurons
GABAergic interneurons
f
Choroid plexus
g
RAMP1
RAMP3
Expression level
h

Figure 3. Single cell transcriptional profiling in control and hypoxia exposed hSO and hCO.

a. UMAP visualization of the resolved single cell RNA-seq data of hSO with assignment of main cell clusters, with control and hypoxia exposure shown by condition (*n[total]* = 16,022 cells, *n[control]* = 8,691 cells, *n[hypoxia]* = 7,331 cells); **b.** UMAP visualization of the resolved single cell RNA-seq data of hCO with assignment of main cell clusters, with control and hypoxia exposure shown by condition (*n[total]* = 12,567 cells, *n[control]* = 6,786 cells, *n[hypoxia]* = 5,781 cells); **c.** Single cell gene expression level (log) of well-established interneuron markers of MGE and CGE origin (*NKX2.1, CALB2, SST, LHX6*) across interneuron subclusters in hSO; **d.** Single cell gene expression level (log) of well-established interneuron markers of MGE and CGE origin (*NKX2.1, CALB2, SST, LHX6*) across interneuron subclusters in hCO; **e.** Single cell gene expression level (log) of adrenomedullin (*ADM*) and main receptor of action (*RAMP2*) in main cell clusters of hSO; **f.** Single cell gene expression level (log) of adrenomedullin (*ADM*) and main receptor of action (*RAMP2*) in main cell clusters of hCO; **g.** Single cell gene expression level of other *RAMP* family receptors (*RAMP1* and *RAMP3*) in main cell clusters of hSO; **h.** Single cell gene expression level (log) of other *RAMP* family receptors (*RAMP1* and *RAMP3*) in main cell clusters of hCO.

FIGURE 4

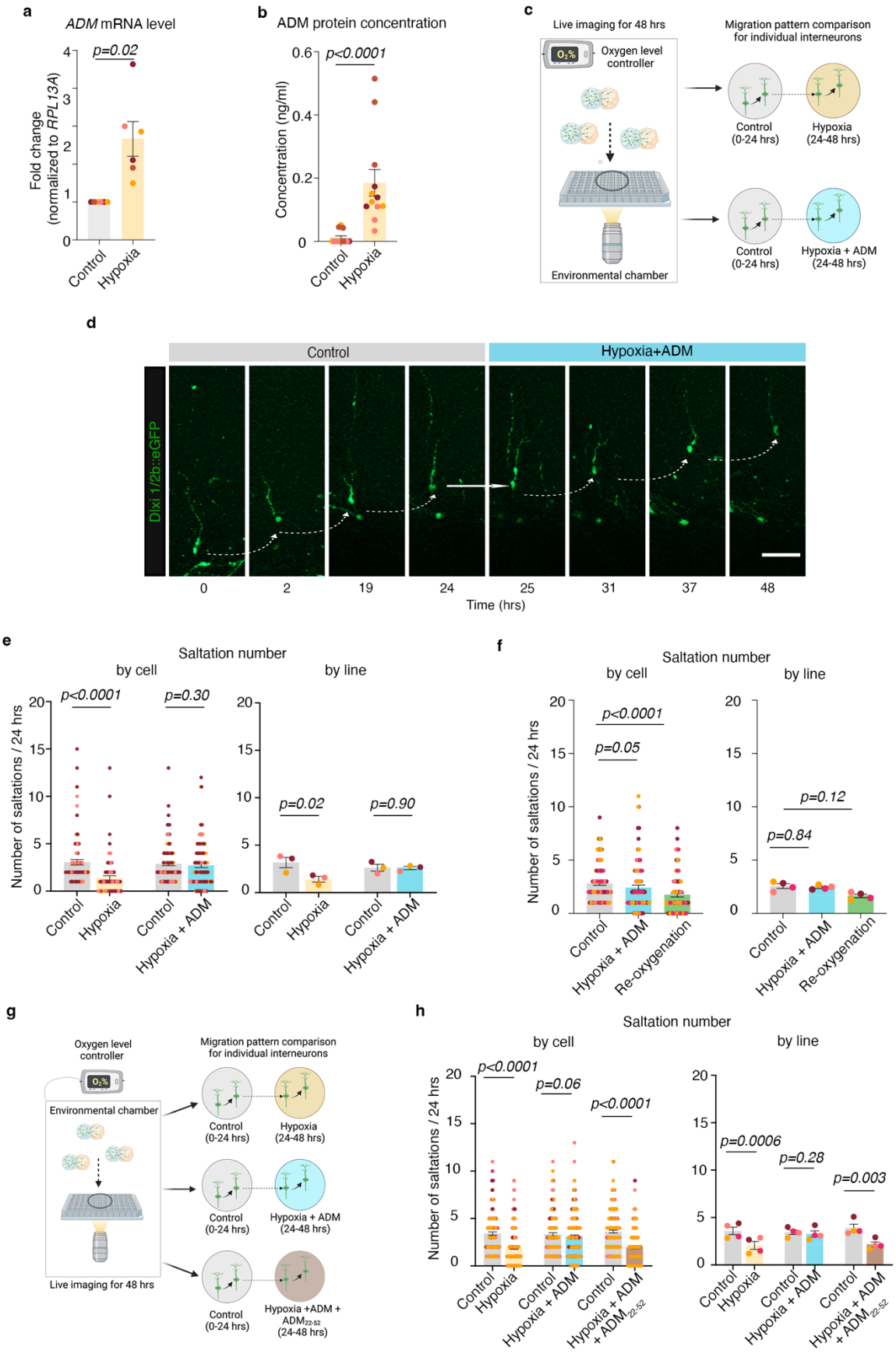
a
ADM mRNA level
p=0.02
Fold change (normalized to RPL13A)
Control
Hypoxia
b
ADM protein concentration
p<0.0001
Concentration (ng/ml)
Control
Hypoxia
c
Live imaging for 48 hrs
Oxygen level controller
Environmental chamber
Migration pattern comparison for individual interneurons
Control (0-24 hrs)
Hypoxia (24-48 hrs)
Control (0-24 hrs)
Hypoxia + ADM (24-48 hrs)
d
Control
Hypoxia+ADM
Dlxi 1/2b::eGFP
0
2
19
24
25
31
37
48
Time (hrs)
e
Saltation number
by cell
by line
p<0.0001
p=0.30
p=0.02
p=0.90
Number of saltations / 24 hrs
Control
Hypoxia
Control
Hypoxia + ADM
f
Saltation number
by cell
by line
p<0.0001
p=0.05
p=0.12
p=0.84
Number of saltations / 24 hrs
Control
Hypoxia + ADM
Re-oxygenation
g
Oxygen level controller
Environmental chamber
Live imaging for 48 hrs
Migration pattern comparison for individual interneurons
Control (0-24 hrs)
Hypoxia (24-48 hrs)
Control (0-24 hrs)
Hypoxia + ADM (24-48 hrs)
Control (0-24 hrs)
Hypoxia +ADM + ADM22-52 (24-48 hrs)
h
Saltation number
by cell
by line
p<0.0001
p=0.06
p<0.0001
p=0.0006
p=0.28
p=0.003
Number of saltations / 24 hrs
Control
Hypoxia
Control
Hypoxia + ADM
Control
Hypoxia + ADM + ADM22-52

Figure 4. Exogenous administration of ADM peptide rescues the migration defects in hypoxia-exposed human cortical interneurons.

a. Transcriptional upregulation (by qPCR) of *ADM* gene in hSO exposed to 24 hrs of hypoxia: *ADM* (two-tailed paired *t*-test, P=0.02); **b.** Quantitative enzyme immunoassay analysis of adrenomedullin (ADM) peptide in media from hSO exposed and non-exposed to hypoxia (unpaired Mann-Whitney U, P<0.0001; for values below the minimal detection range of <0.01 ng/mL, value was approximated to 0 (we had 9 values approximated to 0 in the control samples); **c.** Schematic of experimental design for pharmacological rescue experiments using ADM; 0.5 μM ADM was added to the media at the beginning of hypoxia exposure; **d.** Example of migration pattern for one interneuron in control versus hypoxia + ADM; **e. (Left)** Quantification of saltations number/24 hrs in control versus hypoxia conditions (paired Wilcoxon test, P<0.0001) and in control versus hypoxia + ADM by individual cells (paired Wilcoxon test, P=0.3); **(Right)** Quantification of saltations number/24 hrs in control versus hypoxia conditions (two-tailed paired *t*-test, P=0.02) and in control versus hypoxia + ADM conditions by hiPSC line (two-tailed paired *t*-test, P=0.90); **f. (Left)** Quantification of saltations number/24 hrs in control versus hypoxia + ADM conditions by individual cells (Friedman test, P=0.05) and in control versus re-oxygenation after hypoxia + ADM by individual cells (Friedman test, P<0.0001); 35% decrease compared to 65% decrease when ADM not added to hypoxia; **(Right)** Quantification of saltations number/24 hrs in control versus hypoxia conditions by hiPSC line (one-way ANOVA, P=0.84) and in control versus re-oxygenation after hypoxia + ADM conditions by hiPSC line (one-way ANOVA, P=0.12); **g.** Schematic of experimental design for pharmacological rescue experiments using ADM_{22-52} receptor blocker; **h. (Left)** Quantification of saltations number/24 hrs in control versus hypoxia conditions by individual cells (paired Wilcoxon test, P<0.0001), control versus hypoxia + ADM (paired Wilcoxon test, P=0.06), and control versus hypoxia + ADM + ADM_{22-52} conditions (paired Wilcoxon test, P<0.0001); **(Right)** Quantification of saltations number/24 hrs in control versus hypoxia conditions by hiPSC line (paired *t*-test test, P=0.0006), control versus hypoxia + ADM (paired *t*-test, P=0.28), and control versus hypoxia + ADM + ADM_{22-52} conditions (two-tailed paired *t*-test, P=0.003). Bar charts: mean±s.e.m.. Different dot colors represent individual hiPSC lines.

FIGURE 5

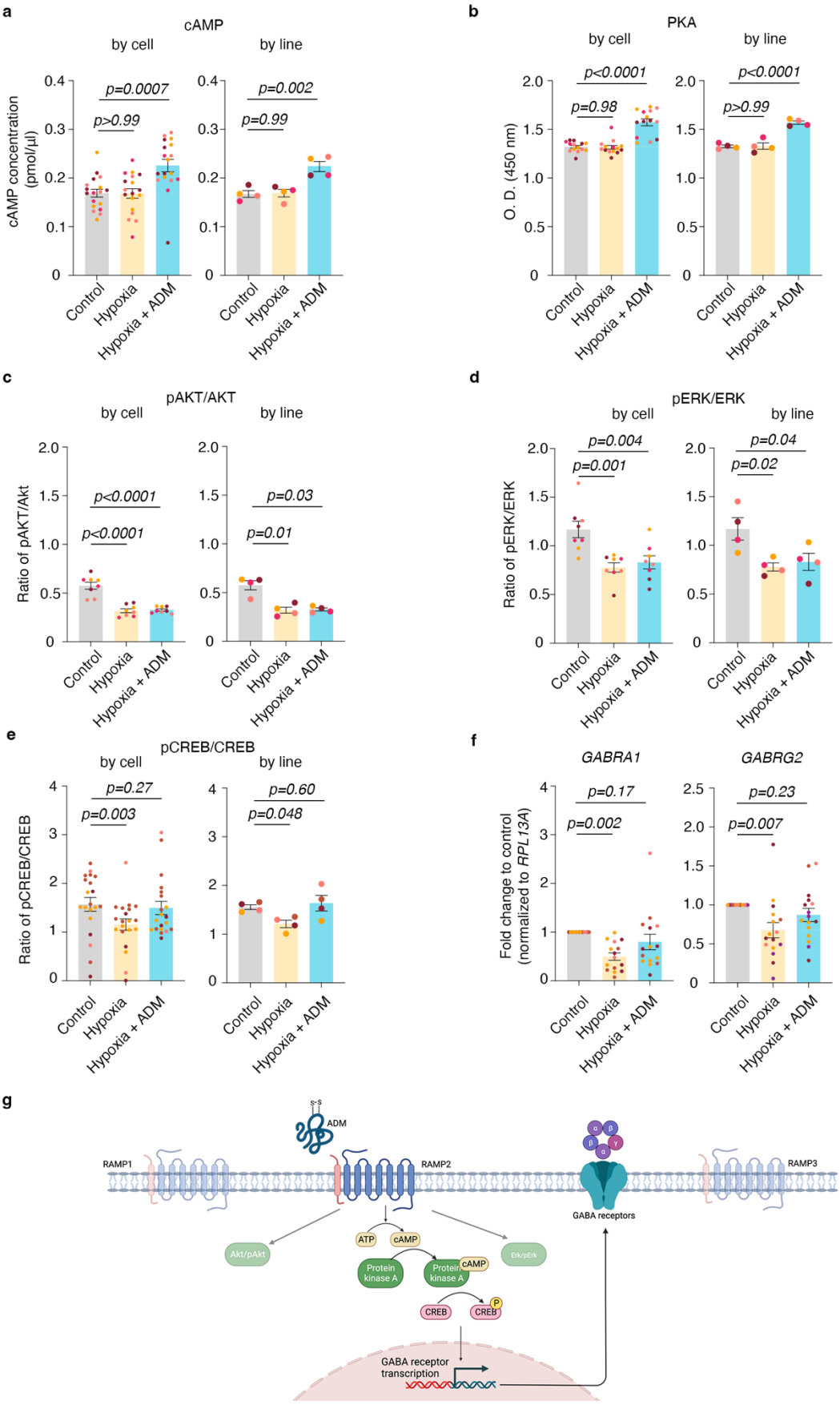
a
cAMP
by cell
by line
cAMP concentration (pmol/µl)
p=0.0007
p>0.99
p=0.002
p=0.99
Control
Hypoxia
Hypoxia + ADM
b
PKA
O. D. (450 nm)
p<0.0001
p=0.98
p<0.0001
p>0.99
c
pAKT/AKT
Ratio of pAKT/Akt
p<0.0001
p<0.0001
p=0.03
p=0.01
d
pERK/ERK
Ratio of pERK/ERK
p=0.004
p=0.001
p=0.04
p=0.02
e
pCREB/CREB
Ratio of pCREB/CREB
p=0.27
p=0.003
p=0.60
p=0.048
f
GABRA1
GABRG2
Fold change to control (normalized to RPL13A)
p=0.17
p=0.002
p=0.23
p=0.007
g
ADM
RAMP1
RAMP2
RAMP3
GABA receptors
Akt/pAkt
ATP
cAMP
Erk/pErk
Protein kinase A
CREB
P
GABA receptor transcription

Figure 5. Molecular mechanism of rescue by ADM

a. (Left) Quantification of cAMP concentration (pmol/µl) by individual hSOs in control versus hypoxia (one-way ANOVA, P>0.99) and, control versus hypoxia + ADM (one-way ANOVA, P=0.0007), **(Right)** Quantification of cAMP concentration (pmol/µl) by hiPSC line in control versus hypoxia (one-way ANOVA, P=0.99) and, control versus hypoxia + ADM (one-way ANOVA, P=0.002); **b. (Left)** Quantification of PKA activity (O.D. 450nm) by individual hSOs in control versus hypoxia (one-way ANOVA test, P=0.98) and control versus hypoxia + ADM (one-way ANOVA, P<0.0001); **(Right)** Quantification of PKA activity (O.D. 450nm) by hiPSC line in control versus hypoxia (one-way ANOVA, P>0.99) and control versus hypoxia + ADM (one-way ANOVA, P<0.0001); **c. (Left)** Quantification of pAKT/AKT by individual hSOs in control versus hypoxia (one-way ANOVA, P<0.0001) and control versus hypoxia + ADM (one-way ANOVA, P<0.0001); **(Right)** Quantification of pAKT/AKT by hiPSC line in control versus hypoxia (Kruskal-Wallis test, P=0.01) and control versus hypoxia + ADM (Kruskal-Wallis test, P=0.03); **d. (Left)** Quantification of pERK/ERK by individual hSOs in control versus hypoxia (one-way ANOVA test, P=0.001) and control versus hypoxia + ADM (one-way ANOVA test, P=0.004); **(Right)** Quantification of pERK/ERK by hiPSC line in control versus hypoxia (one-way ANOVA test, P=0.02) and control versus hypoxia + ADM (one-way ANOVA test, P=0.04); **e. (Left)** Quantification of pCREB/CREB by individual hSOs in control versus hypoxia (one-way ANOVA test, P=0.003) and control versus hypoxia + ADM (one-way ANOVA test, P=0.27); **(Right)** Quantification of pCREB/CREB by hiPSC line in control versus hypoxia (one-way ANOVA test, P=0.048) and control versus hypoxia + ADM (one-way ANOVA test, P=0.6) **f. (Left)** Quantification (by q-PCR) of GABRA1 in individual hSOs in control versus hypoxia conditions (one-way ANOVA test, P=0.002) and control versus hypoxia + ADM (one-way ANOVA test, P=0.17); **(Right)** Quantification (by q-PCR) of GABRG2 in individual hSOs in control versus hypoxia conditions (one-way ANOVA test, P=0.007) and control versus hypoxia + ADM (one-way ANOVA test, P=0.23); **g.** Schematic of proposed molecular mechanism of rescue by ADM. Bar charts: mean±s.e.m. Different dot colors represent individual hiPSC lines.

FIGURE 6

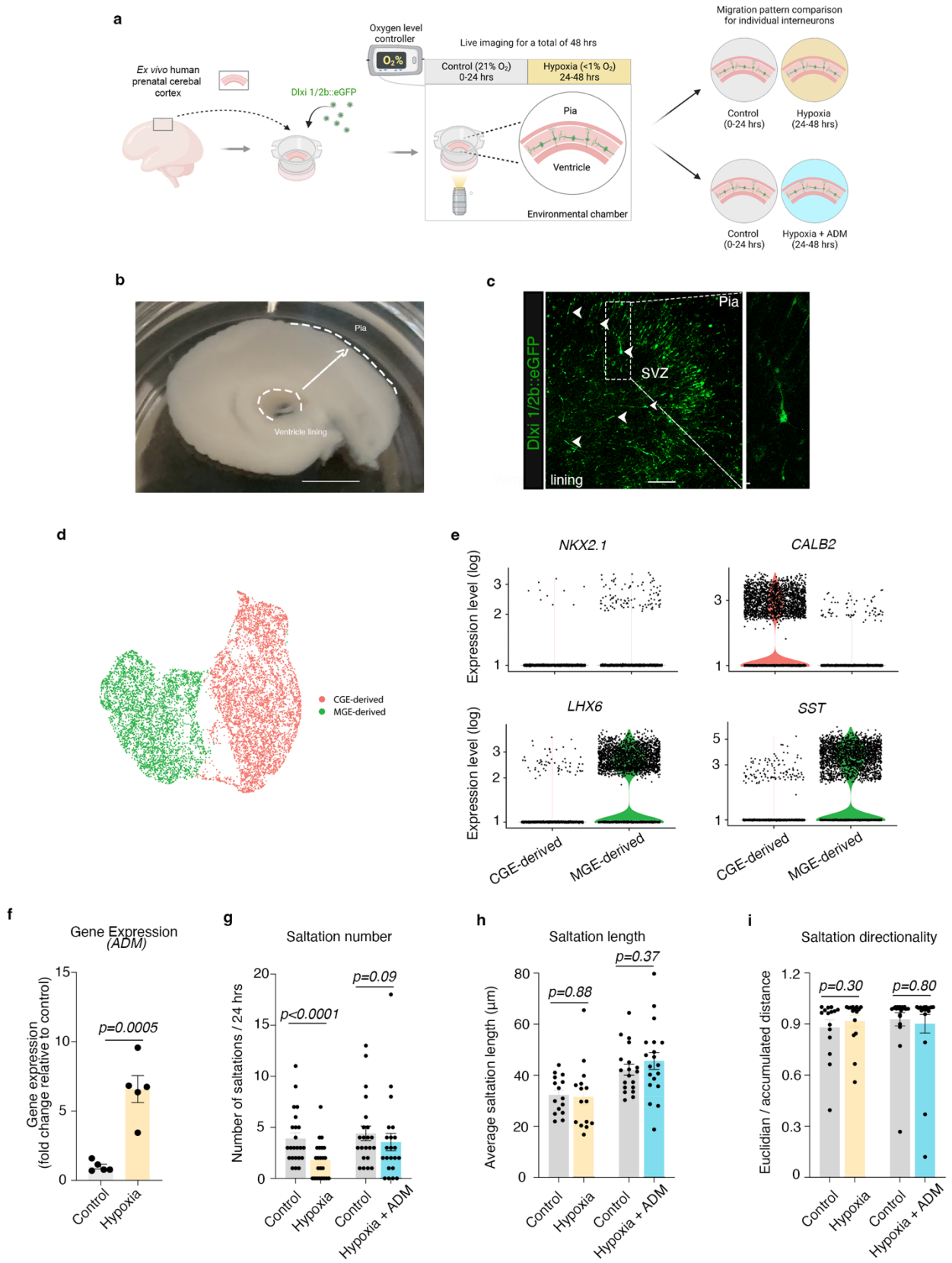
a
Ex vivo human prenatal cerebal cortex
Dlxi 1/2b::eGFP
Oxygen level controller
Live imaging for a total of 48 hrs
Control (21% O2) 0-24 hrs
Hypoxia (<1% O2) 24-48 hrs
Pia
Ventricle
Environmental chamber
Migration pattern comparison for individual interneurons
Control (0-24 hrs)
Hypoxia (24-48 hrs)
Control (0-24 hrs)
Hypoxia + ADM (24-48 hrs)
b
Pia
Ventricle lining
c
Pia
SVZ
Dlxi 1/2b::eGFP
lining
d
CGE-derived
MGE-derived
e
NKX2.1
CALB2
LHX6
SST
Expression level (log)
CGE-derived
MGE-derived
f
Gene Expression (ADM)
Gene expression (fold change relative to control)
p=0.0005
Control
Hypoxia
g
Saltation number
Number of saltations / 24 hrs
p<0.0001
p=0.09
Control
Hypoxia
Control
Hypoxia + ADM
h
Saltation length
Average saltation length (µm)
p=0.88
p=0.37
Control
Hypoxia
Control
Hypoxia + ADM
i
Saltation directionality
Euclidian / accumulated distance
p=0.30
p=0.80
Control
Hypoxia
Control
Hypoxia + ADM

Figure 6. Migration defect and rescue by ADM in an *ex vivo* model using human prenatal cerebral cortex at mid-gestation.

a. Schematic illustrating the overall experimental design: sections of *ex vivo* human cerebral cortex were collected and initially sectioned at ~3 mm and subsequently at 400 µm thickness; sections were transferred onto cell culture membrane inserts suspended in culture media; for visualization tissue was transfected with Dlxi1/2b::eGFP lentivirus, and imaged 7-10 days post infection directly on inserts; GFP-tagged *ex vivo* human prenatal cortical interneurons were monitored for 24 hrs in control conditions and 24 hrs in hypoxic conditions in the presence or absence of 0.5 µM ADM; **b.** Example of macroscopic view of a 3mm section of fresh *ex vivo* human prenatal cerebral cortex; scale bar: 1 cm; **c.** Representative image of fluorescently-tagged cortical interneurons in a section of *ex vivo* human prenatal cerebral cortex; **d.** UMAP for GABAergic interneurons subtype clustering from previously published databases on mid-gestation fetal tissue (MGE and CGE); **e**. Single cell gene expression level (log) of the well-established genes present in interneurons of MGE and CGE origin (e.g. *NKX2.1, LHX6, SST, CALB2*) across the interneuron subclusters; **f.** Transcriptional increase of *ADM* gene following 24 hrs of exposure to hypoxia of *ex vivo* human prenatal cerebral cortex samples (two-tailed unpaired *t*-test, P=0.0005); **g.** Quantification of saltation numbers/24 hrs in control versus hypoxia conditions (paired Wilcoxon test, P<0.0001) and control versus hypoxia + ADM conditions by individual cells (paired Wilcoxon test, P=0.09); **h.** Quantification of average saltation length for control versus hypoxia conditions (paired Wilcoxon test, P=0.88) and control versus hypoxia + ADM by individual cells (two-tailed paired *t*-test, P=0.37); **i.** Quantification of directionality of migration for control versus hypoxia conditions (paired Wilcoxon test, P=0.3) and control versus hypoxia + ADM by individual cells (paired Wilcoxon test, P=0.8). Bar charts: mean±s.e.m; scale bars: 1cm, 200 µm and 50 µm.

EXTENDED FIGURE 1

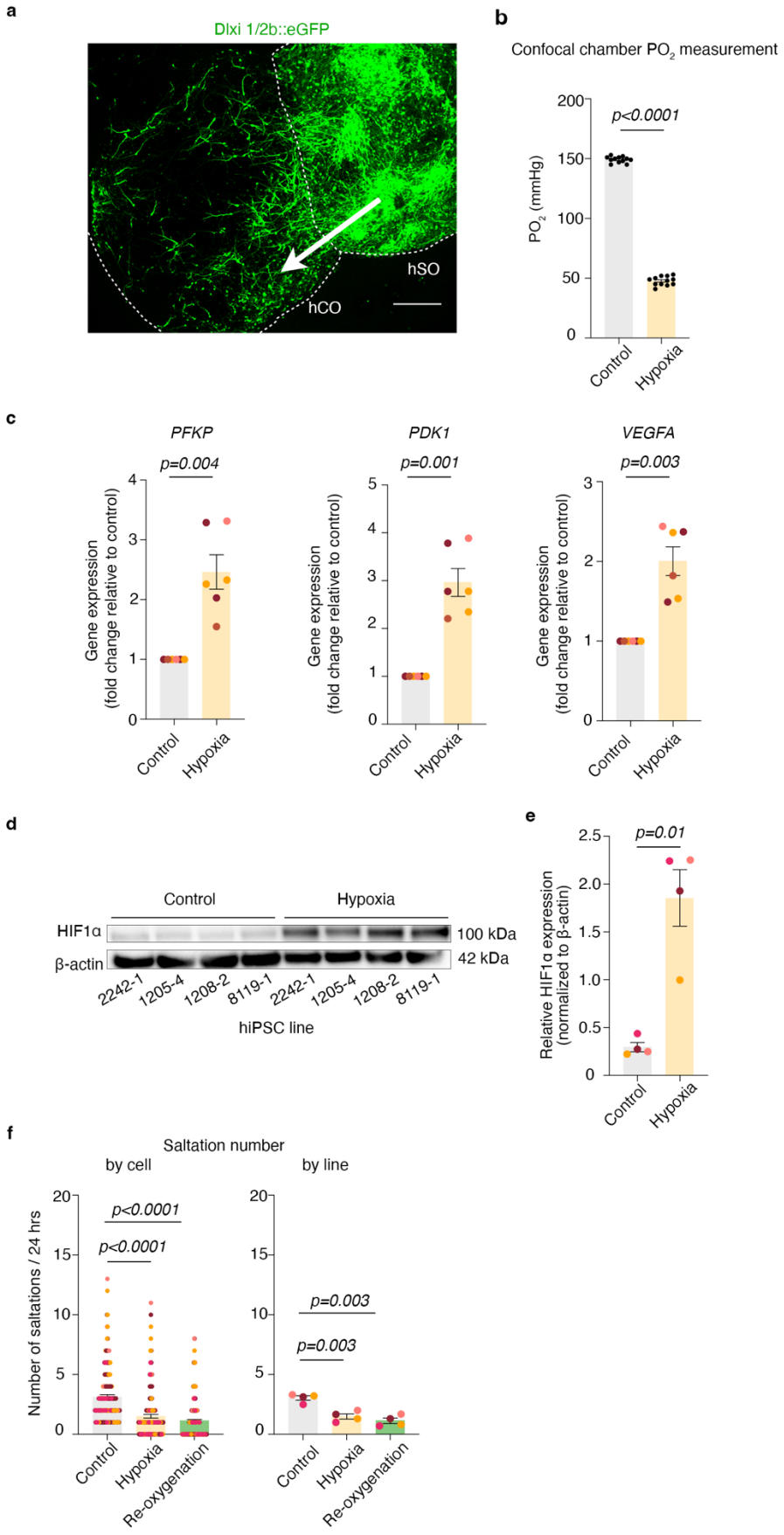

Extended Figure 1. Example of hFA, oxygen level measurements in the confocal chamber and qPCR changes in expression of hypoxia-responsive genes.

a. Example image of hFA showing cortical interneurons migrated from the hSO side to the hCO side; arrow indicates the direction of migration from hSO to hCO; **b.** Oxygen levels (PO_2 (mmHg)) in cell culture media under control conditions and following exposure to hypoxia for 24 hrs in the confocal microscope environmental chamber (unpaired *t*-test, P<0.0001); **c.** Transcriptional upregulation of hypoxia-responsive genes in hSO exposed to 24 hrs of hypoxia (<1% O_2): *PFKP* (two-tailed paired *t*-test, P=0.004), *PDK1* (two-tailed paired *t*-test, P=0.001), *VEGFA* (two-tailed paired *t*-test, P=0.003); **d.** Example of Western Blot showing the stabilization of HIF1α protein in hSOs from 4 hiPSC lines upon exposure to hypoxia, and β-actin expression for normalization; **e**. Quantification of HIF1α protein, normalized to β-actin (two-tailed paired *t*-test; P=0.01); **f. (Left)** Quantification of saltations number/24 hrs by individual cells in control versus hypoxia (Friedman test, P<0.0001) and control versus re-oxygenation (Friedman test, P<0.0001); **(Right)** Quantification of saltations number/24 hrs in by hiPSC line in control versus hypoxia (one-way ANOVA, P=0.003) and control versus re-oxygenation (one-way ANOVA, P=0.003). Bar charts: mean ± s.e.m; scale bar: 200 µm.

EXTENDED FIGURE 2

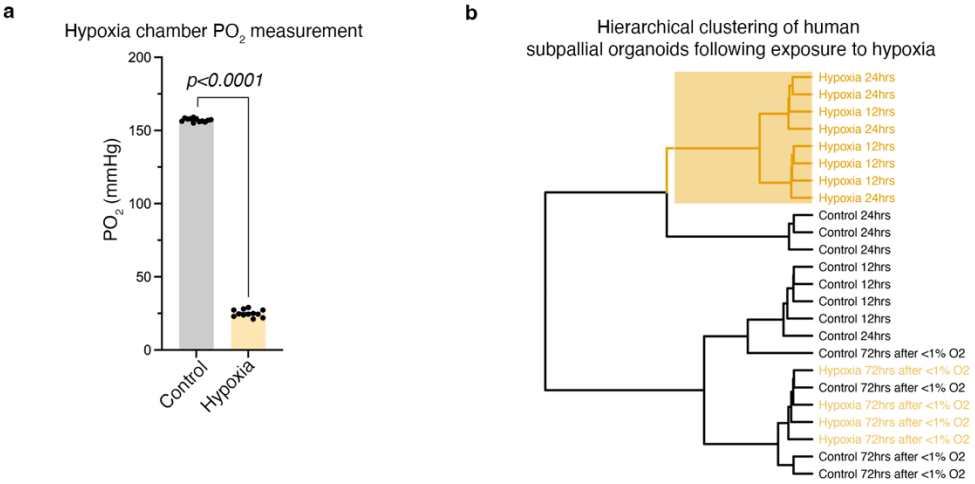

Extended Figure 2. Oxygen level measurements for RNA-Sequencing experiments and dendrogram of sample clustering.

a. Oxygen levels (PO_2 (mmHg)) in cell culture media under control conditions and following exposure to hypoxia for 24 hrs in the C-chamber hypoxia sub-chamber (Biospherix) (unpaired *t*-test, $P<0.0001$); **b.** Hierarchical clustering, using Ward's criterion, of the first three principal components of the normalized gene expression profiles of all 17,777 genes passing quality control shows clear separation of 12 and 24 hrs hypoxia-exposed samples versus control and from reoxygenated samples. Bar charts: mean±s.e.m.

EXTENDED FIGURE 3

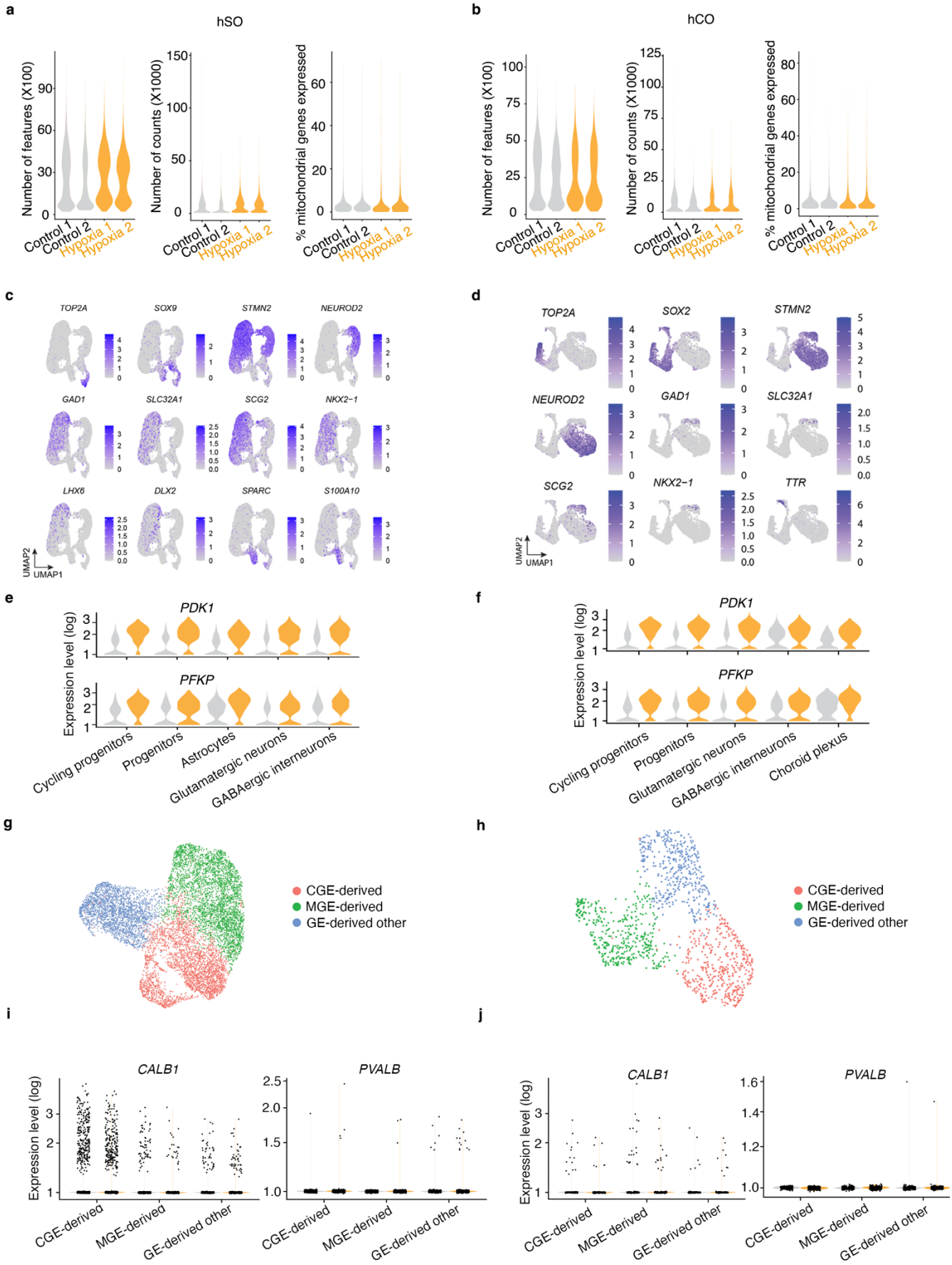

Extended Figure 3. Quality control and robustness analyses for scRNA-sequencing data

a. (Left) Reconstruction of variable features (x100), **(Middle)** number of counts, and **(Right)** percentage of mitochondrial genes expressed, across biological replicates for both control and hypoxia exposed, hSOs separated from hFAs; **b. (Left)** Reconstruction of variable features (x100), **(Middle)** number of counts, and **(Right)** percentage of mitochondrial genes expressed, across biological replicates for both control and hypoxia exposed, hCOs separated from hFAs; **c.** UMAP visualization of main cellular subclusters in hSOs with corresponding gene expression including, astrocytes (*SPARC, S100A10*), progenitors (*SOX9*), cycling progenitors (*SOX9, TOP2A*), glutamatergic neurons (*STMN2, NEUROD2*), interneuron progenitors (*NKX2.1, LHX6, DLX2*), and interneurons (*STMN2, GAD1, SLC32A1, SCG2*); **d.** UMAP visualization of main cellular subclusters in hCO with corresponding gene expression including, choroid plexus (*TTR)*, progenitors (*SOX2*), cycling progenitors (*SOX2, TOP2A*), glutaminergic neurons (*STMN2, NEUROD2*), interneuron progenitors (*NKX2.1*), and interneurons (*STMN2, GAD1, SLC32A1, SCG2*); **e**. Single cell gene expression level (log) of hypoxia-responsive genes (*PDK1* and *PFKP*) across main cellular subclusters in hSO; **f.** Single cell gene expression level (log) of hypoxia-responsive genes (*PDK1* and *PFKP*) across main cell clusters in hCO; **g.** UMAP for GABAergic interneurons subtype clustering as defined in main figure 3 (CGE and MGE) in hSO; **h.** UMAP for GABAergic interneurons subtype clustering as defined in main figure 3 (CGE and MGE) in hCOs; **i.** Single cell gene expression level (log) of additional interneuron markers (*CALB1* and *PVALB*) MGE and CGE interneurons across hSOs; **j.** Single cell gene expression level (log) of additional interneuron markers (CALB1 and *PVALB*) MGE and CGE interneurons across hCOs.

EXTENDED FIGURE 4

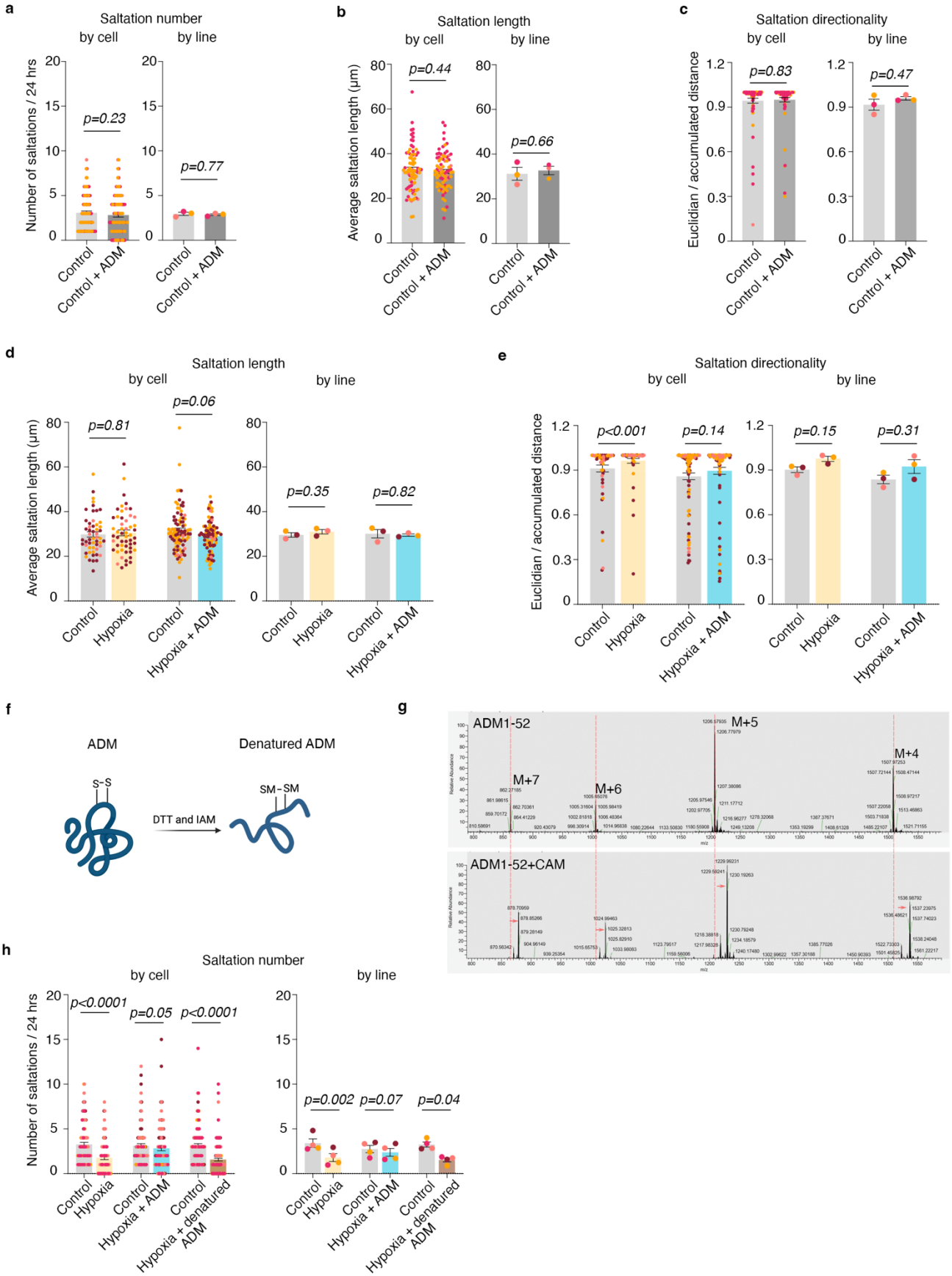

Extended Figure 4. Rescue by ADM.

a. (Left) Quantification of saltations number/24 hrs in control versus control + ADM conditions by individual cells (paired Wilcoxon test, P=0.23); **(Right)** Quantification of saltations number/24 hrs in control versus control + ADM conditions by hiPSC line (two-tailed paired *t*-test, P=0.77); **b. (Left)** Quantification of average saltation length in control versus control + ADM conditions by individual cells (two-tailed paired *t*-test, P=0.44); **(Right)** Quantification of average saltation length in control versus control + ADM conditions by hiPSC line (two-tailed paired *t*-test, P=0.66); **c. (Left)** Quantification of directionality of migration in control versus control + ADM conditions by individual cells (paired Wilcoxon test, P=0.83); **(Right)** Quantification of directionality of migration in control versus control + ADM conditions by hiPSC line (two-tailed paired *t*-test, P=0.47); **d. (Left)** Quantification of average saltation length for control versus hypoxia conditions by individual cells (paired Wilcoxon test, P=0.81) and control versus hypoxia + ADM conditions by individual cells (P=0.06); **(Right)** Quantification of average saltation length for control versus hypoxia conditions by hiPSC line (two-tailed paired *t*-test, P=0.35) and, control versus hypoxia + ADM conditions by hiPSC line (two-tailed paired *t*-test, P=0.82); **e. (Left)** Quantification of directionality of migration for control versus hypoxia conditions by individual cells (paired Wilcoxon test, P<0.001), control versus hypoxia + ADM by individual cells (paired Wilcoxon test, P=0.14); **(Right)** Quantification of directionality of migration for control versus hypoxia conditions by hiPSC line (two-tailed paired *t*-test, P=0.15) and control versus hypoxia + ADM by hiPSC line (two-tailed paired *t*-test, P=0.31); **f.** Schematic of denaturing procedure for ADM, including reduction and alkylation using dithiothreitol (*DTT*) and iodoacetamide (*IAM*), resulting in carbamidomethylated (*CAM*) cysteines at Cys16 and Cys21; **g.** LC-MS based analysis of the non-modified ADM (top) and the denatured ADM form (bottom), displays characteristic M+4 through M+7 peaks with two CAM modifications (+114 Da) in the bottom panel represented by the peak shift (arrow); **h.** (**Left)** Quantification of saltations number/24 hrs in control versus hypoxia by individual cells (paired Wilcoxon test, P<0.0001), control versus hypoxia + ADM (paired Wilcoxon test, P=0.05) and control versus hypoxia + denatured ADM (paired Wilcoxon test, P<0.0001); **(Right)** Quantification of saltations number/24 hrs in control versus hypoxia by hiPCS line (two-tailed paired *t*-test, P=0.002, control versus hypoxia + ADM (two-tailed paired *t*-test, P=0.07) and control versus hypoxia + denatured ADM (two-tailed paired *t*-test, P=0.04). Bar charts: mean ± s.e.m.

EXTENDED FIGURE 5

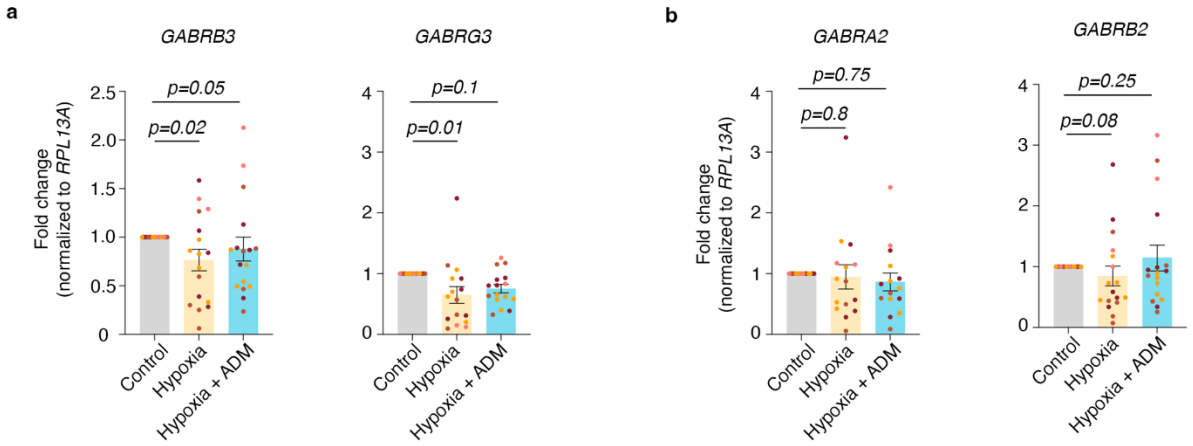

Extended Figure 5. Additional data to support molecular mechanism of rescue by ADM

a. (Left) Quantification (by q-PCR) of GABRB3 in individual hSOs in control versus hypoxia conditions (Kruskal-Wallis test, P=0.02) and control versus hypoxia + ADM (Kruskal-Wallis test, P=0.05); **(Right)** Quantification (by q-PCR) of GABRG3 in individual hSOs in control versus hypoxia conditions (one-way ANOVA test, P=0.01) and control versus hypoxia + ADM (one-way ANOVA test, P=0.1); **b. (Left)** Quantification (by q-PCR) of GABRA2 in individual hSOs in control versus hypoxia conditions (one-way ANOVA, P=0.8) and control versus hypoxia + ADM (one-way ANOVA, P=0.75); **(Right)** Quantification (by q-PCR) of GABRB2 in individual hSOs in control versus hypoxia conditions (Kruskal-Wallis test, P=0.08) and control versus hypoxia + ADM (Kruskal-Wallis test, P=0.25). Bar charts: mean±s.e.m. Different dot colors represent individual hiPSC lines.

EXTENDED FIGURE 6

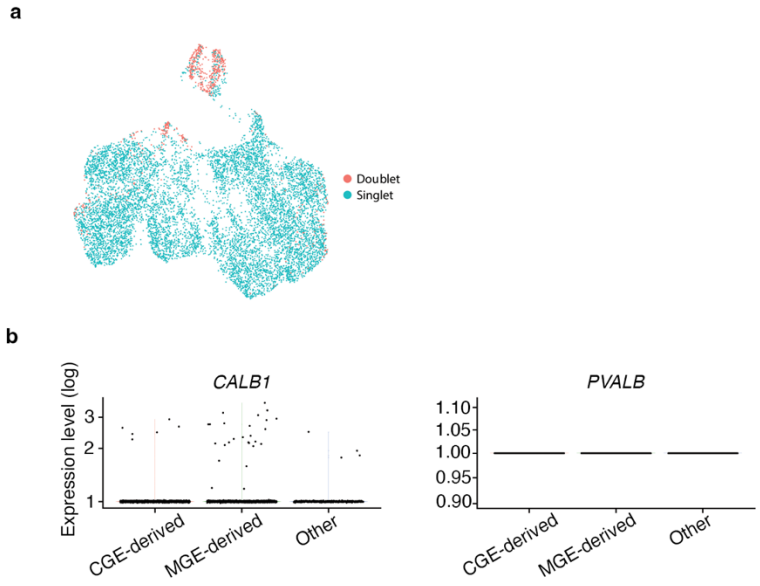

Extended Figure 6. Additional gene expression data from sc-RNAseq.

a. UMAP showing three clusters, including a MGE cluster, a CGE cluster and a third cluster represented by doublets; **b.** Graphical representation of expression of genes associated with GABAergic interneurons subtypes, including *CALB1* and *PVALB*.

Extended Table 1. List of hiPSC lines and number of cells used for each experiment.

Extended Table 2. List of primers used for qPCRs.

Extended Table 3. List of differentially expressed genes by RNA-Sequencing in hSOs exposed to hypoxia.

Extended Table 4. List of GSEA terms from RNA-Sequencing.